ASSESSMENT OF THE PBL-FLOW IN THE EC-MODEL

M. Tiedtke
ECMWF

The ECMWF forecast model has been run operationally now for over two years. Assessment of the forecasts has revealed systematic deficiencies in the simulated flow which are documented in various papers (for example, Tiedtke (1980)). Some of these deficiencies point to erroneous diabatic forcing of the model's flow and, in particular, to that associated with energy exchanges between the atmosphere and ocean/earth. The need for a more detailed assessment of the boundary layer flow, therefore, has become increasingly apparent. This paper presents preliminary results obtained in diagnostic studies of the boundary layer flow in the EC-model.

1. THE PARAMETERIZATION SCHEME OF THE EC-MODEL

The parameterization scheme of the EC-model is described in detail elsewhere, (Tiedtke et al. (1979)), and is therefore only reviewed in relation to boundary layer processes.

The vertical structure of the boundary layer is explicitly resolved, although by only 3 layers, i.e. by a surface layer of 30 m. depth and 2 more layers below 1000 m.

The turbulent processes in the surface layer are simulated by means of the MONIN-OBUKHOV similarity theory where the universal stability dependent functions ϕ for momentum, heat and moisture are expressed in terms of the Richardson number. Although the MONIN-OBUKHOV similarity theory is now generally accepted its use in numerical models may be questionable due to the fact that a general form of the functions ϕ must hold for very different conditions. In fact, no unique mathematical expression for the function ϕ has yet been deduced from observational data (see, for example, Pruitt et al. (1973), where several different expressions of ϕ are discussed).

Above the surface layer the turbulent fluxes are parameterized by an eddy diffusion process based on the mixing length theory. Due to lack of data the diffusion coefficients are assumed to depend on windshear and thermal stability in the same way as for the surface layer. For the special case of free convection the specified height dependency of the diffusion coefficient is supported by observational data (HSU (1973)).

The parameterization of cloud/radiation processes is very crude. No direct radiation/cloud feedback is considered as

(1) the cloud-cover for the radiation calculation is simply specified as a function of the grid-scale relative humidity

(2) clouds fill whole model layers i.e. thin stratiform clouds are not considered

(3) radiative fluxes are calculated in model layer intervals only, preventing a realistic condensation-radiation feedback at cloud tops.

For these reasons clouds at the top of a well mixed boundary layer, which recently gained much attention, are not adequately parameterized in the EC-model.

The parameterization of the boundary layer flow in the presence of cumulus convection is also greatly simplified. The convection scheme used in the EC-model is a moisture convergence scheme based on Kuo's proposal (Kuo (1974)). The interface of the convective flow and the boundary layer flow occurs therefore mainly through the moisture convergence within the lower levels. Effects such as cumulus induced subsidence within the environmental air, downdrafts and momentum transport are neglected altogether.

2. ASSESSMENT OF THE PBL

Verification of the boundary layer flow in large scale numerical models is difficult for various reasons, two of which shall be mentioned here.

A principle problem arises from the assumption of homogeneity of the underlying surface within a gridsquare in numerical models. Since irregularities of the earth's surface strongly influence the near surface flow, a verification of the boundary layer flow as simulated in large-scale models against the observed flow given at single stations seems extremely difficult over land and, in particular, near mountains.

The second point is related to our present data assimilation scheme. Observational data are assimilated at main pressure levels which are far apart in the lower troposphere, i.e. the next level above the 1000 mb level is the 850 mb pressure surface. Thus, observational data describing the boundary layer flow and its vertical structure are neglected altogether. Although it is not clear if the lack of these data will significantly affect the forecast quality as the initial boundary layer flow is presumably readjusted in the forecast to the model's internal boundary layer flow. However, the verification of the boundary layer would benefit from assimilating the boundary layer flow. As the boundary layer flow presently cannot be verified we can only assess the simulated boundary layer flow.

2.1 Global mean flow

As has already been known for some time, the flow simulated in the EC-model has some systematic deficiencies when compared with the observed flow. In the context of this workshop, the most noticeable deficiencies are:

(1) The tendency to cool the model's atmosphere by several K. This cooling is due to an imbalance of the radiative cooling on the one side and the energy supply in the form of sensible and latent heat on the other side (Fig. 1). In view of the lower rate of radiative cooling as compared to the estimated real value of 100 W/m^2 the net cooling must be due to an underestimate of the net surface energy flux into the atmosphere by probably as much as 20 W/m^2.

(2) A considerably higher rate of the internal energy conversion than observed. This is concluded from comparing the conversion rates at the later stage of an extended integration, when the model has reached its own equilibrium, against the initial conversion rate, which is presumably close to reality (Fig. 2). The increase is nearly 40% of its initial value and appears simultaneously in the dissipation rate due to vertical diffusion of momentum (with the largest contribution from the boundary layer). The total kinetic energy is, as we conclude also from Fig. 2, well preserved in time, although the kinetic energy of the zonal flow has increased at the cost of the eddy kinetic energy.

Monthly mean boundary layer flow for April 1981

We next consider the time averaged boundary layer flow and compare the initial flow as given by our data assimilation and the mean flow of all 10-day forecasts for April, 1981. With regard to the initial flow we must remember that observational data within the lower atmosphere, i.e. between 1000 mb and 850 mb are presently not considered in our data assimilation. The initial boundary layer flow is therefore essentially the model-generated flow in the presence of external forcing as by horizontal pressure gradient, the earth's rotation, baroclinicity, thermal stratification and surface conditions.

The mean flow at the top of the surface layer (= lowest model level at 30m above ground) appears realistic (Fig. 3), as the main circulation patterns like tradewinds, mid-latitudinal westerlies, and stationary large-scale vortices, as well as the weak surface wind over the continents are captured, both in the initial and in the predicted mean flow. The windspeed of the mean flow is largest along the cyclone tracks in the Southern Hemisphere where it locally exceeds 12 m/sec in the forecasts (Fig. 4). It increased there during the forecast by 2 m/sec on average. The surface winds are, presumably, larger

on average than observed, as the climatic geostrophic winds at sea levels for April hardly exceed 12 m/sec. (Jenne et al., 1971). Strong surface mean winds of 6 m/sec appear also along the Northern Hemispheric cyclone tracks, which increase during the forecast mainly over the eastern parts. In the tradewind region the mean surface wind is 6 m/sec and it decreased during the forecasts by about 2 m/sec.

As mentioned before, a verification of the surface wind is not possible for this particular month, but we compared the simulated mean flow with the mean climate surface wind for April over the Tropical Atlantic and the Eastern Pacific (Hastenrath and Lamb, 1977, Chart 17) and over the Indian Ocean (Hastenrath and Lamb, 1979, Chart 17). Although a direct comparison is not possible as the model's values and the observed values refer to different heights above ground (30 m against 10 m), we found:

(a) close agreement in the location of the extreme values with the climate , but

(b) a much smoother wind field in the simulation; i.e. strong winds are reduced and weak winds are increased in strength, and practically no areas of calm exist.

The windshear in the boundary layer above the surface layer (considered as the depth of two model layers extending from h = 30m to h = 800m) is much smaller than in the surface layer (Fig. 5). In the Southern Hemispheric westerlies it approaches 6 m/sec on 770m. In the tropics and subtropics, the shear stays below 2 m/sec everywhere except over the Andes, parts of Africa and South China. During the forecasts the shear of the mean flow decreased over most of the tropics and subtropics, over large areas, by more than 2 m/sec. The simulated flow is again not verified for this month. It agrees qualitatively with the observed mean flow over the tropical oceans. According to Augstein (1978), who summarized the present knowledge about the kinematic and thermodynamic structure of the tropical boundary layer, the windshear is indeed concentrated in the surface layer and is much smaller and occasionally negative above. However, large variations exist depending on the geostrophic flow, the thermal wind, convective activity, etc. Detailed diagnostic studies (probably case studies) are therefore needed for different synoptic conditions.

The thermodynamic structure of the boundary layer is determined by its content of heat and water vapour and by its thermal stability which, in the cloud free boundary layer, is equivalent to the vertical gradient of the virtual potential temperature.

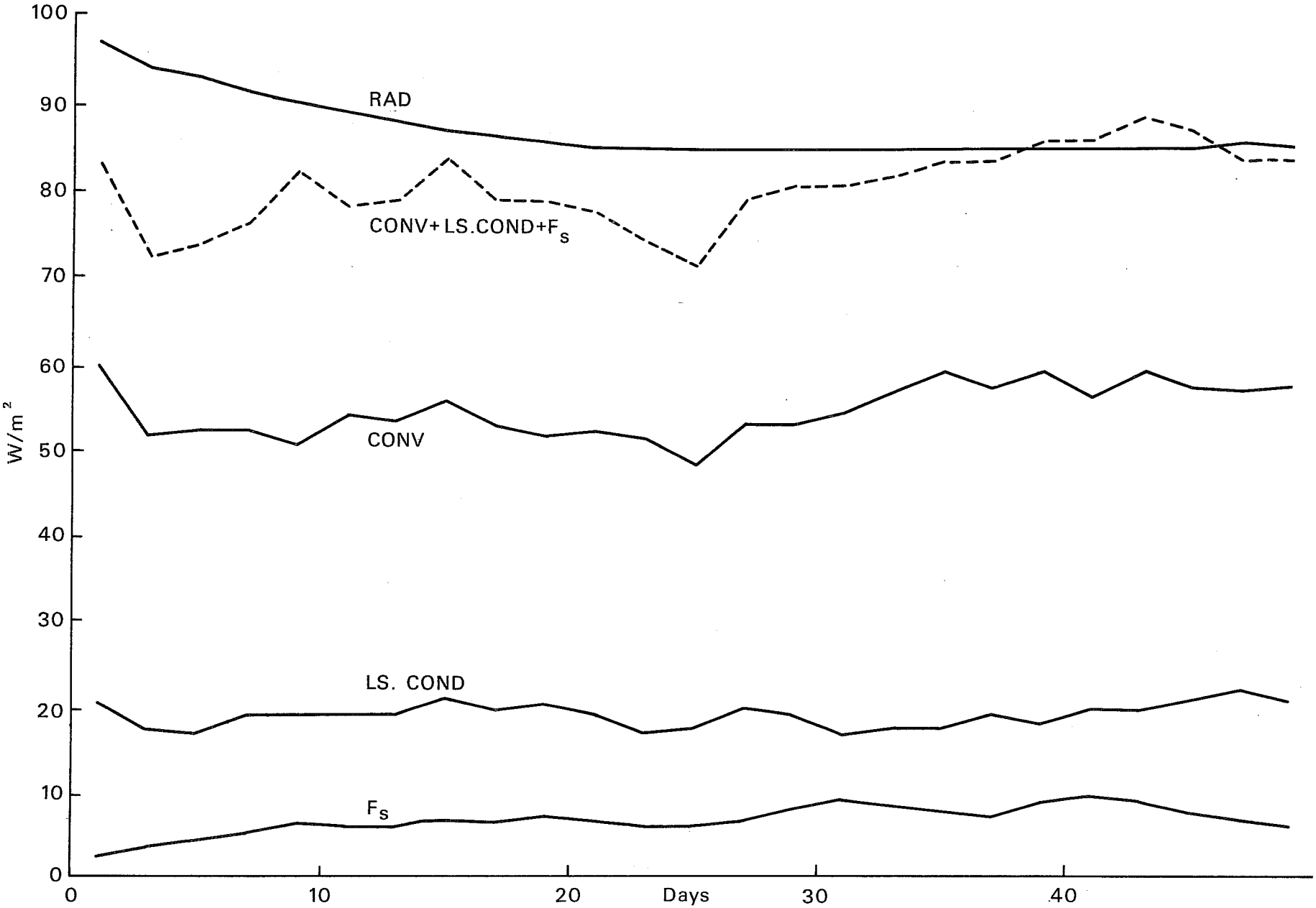

Fig. 1 Time evolution of global mean diabatic heating rates due to radiation, convection, large-scale condensation and surface heat exchange in a winter simulation experiment (B52).

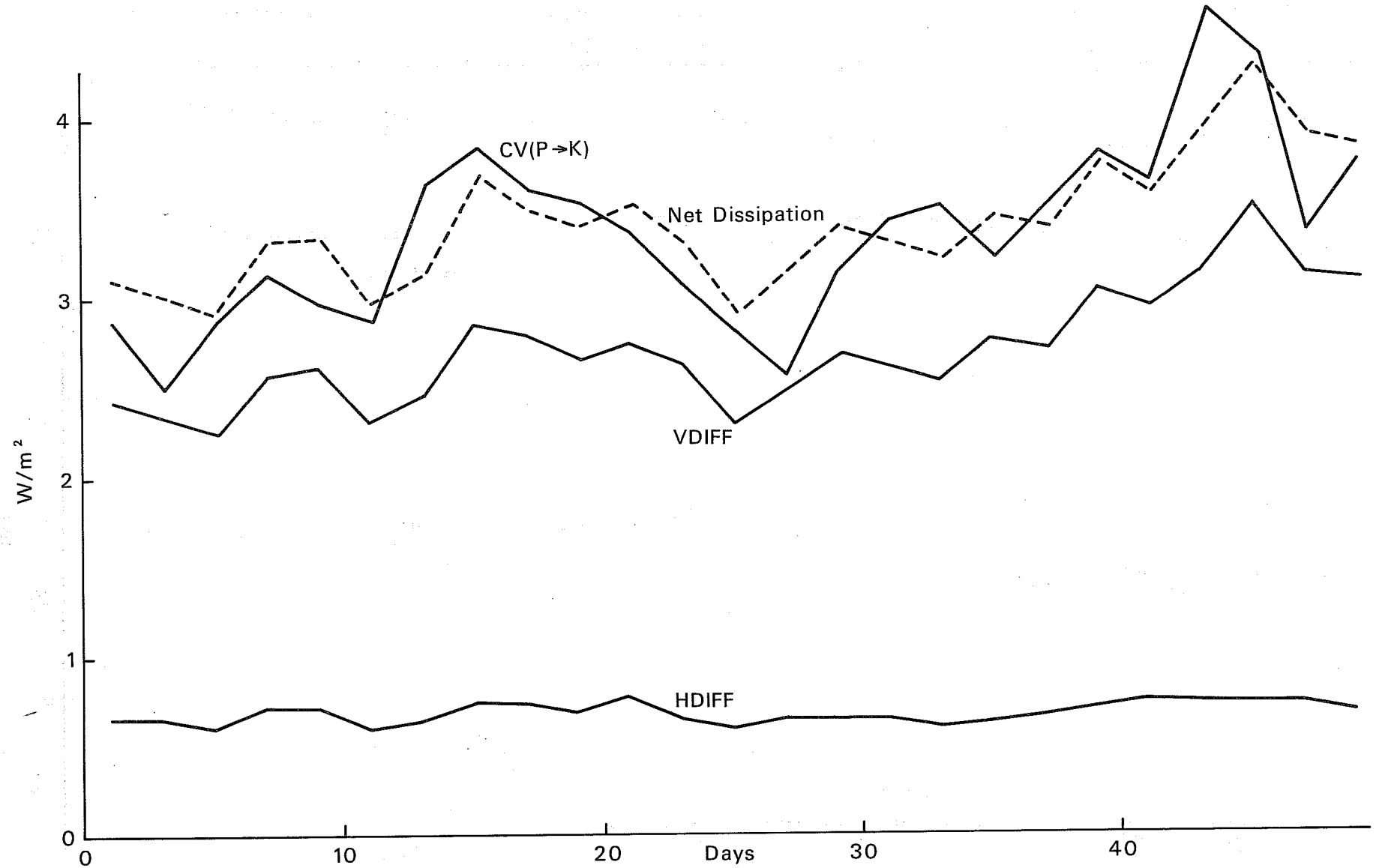

Fig. 2 Time evolution of global mean rates of energy conversion and loss of kinetic energy due to vertical and horizontal momentum diffusion.

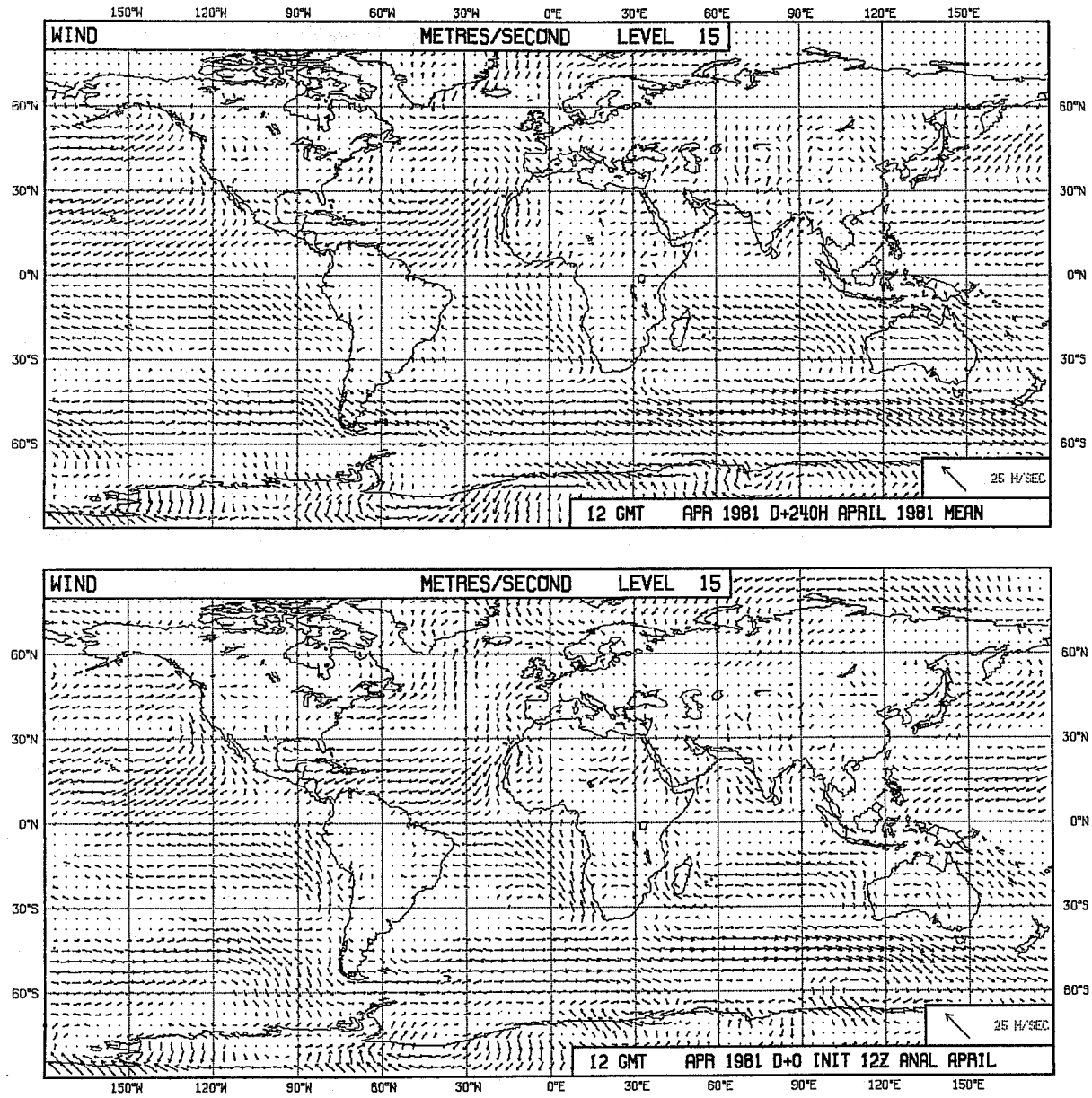

Fig. 3 Mean surface wind vectors (at h=30 m) of all operational EC-forecasts in April 1981 at t=10 d (upper figure) and initially (lower figure).

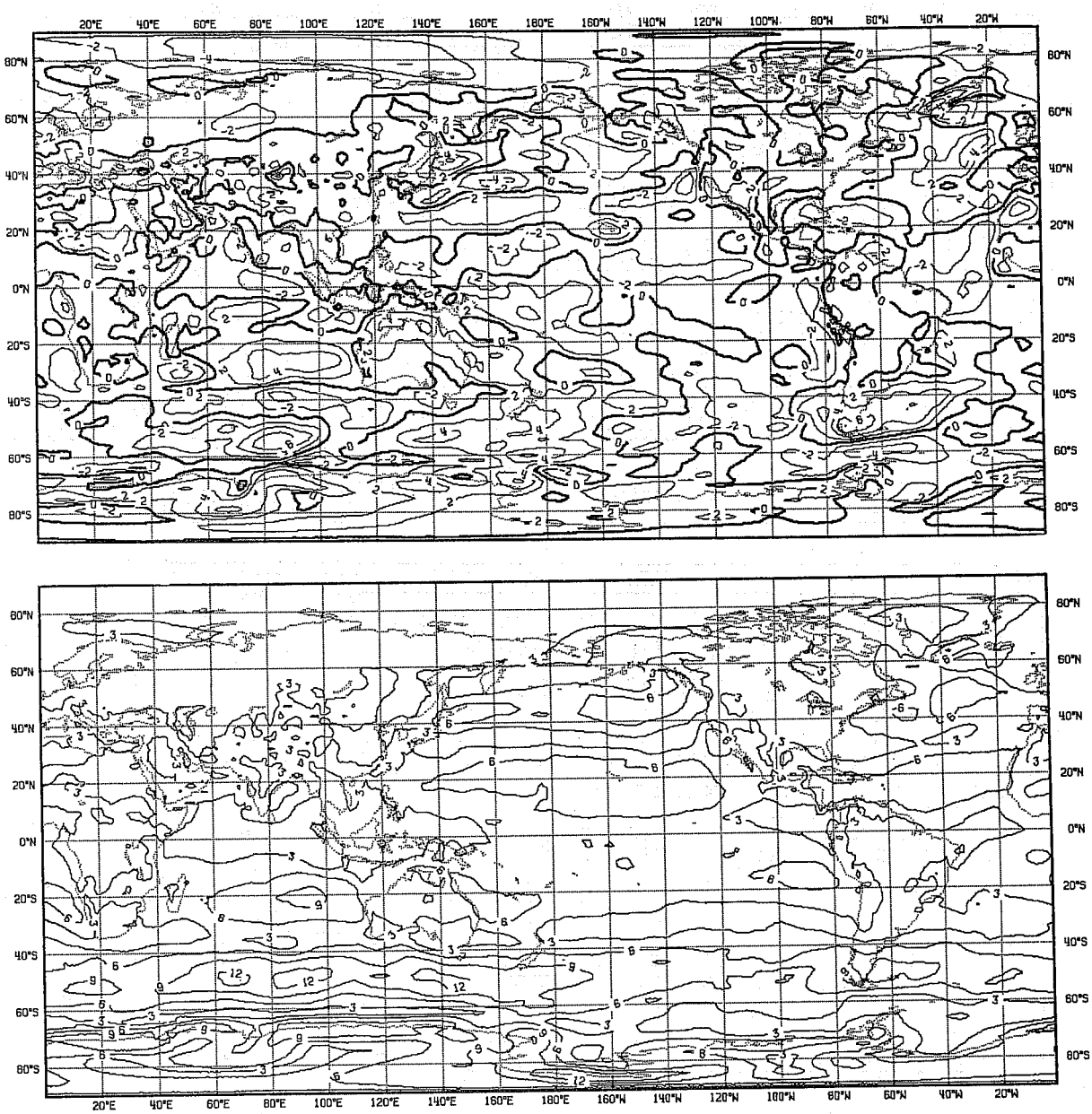

Fig. 4 Mean surface wind speed (at h=30 m) of all operational EC-forecasts in April 1981 at day 10 (lower figure) and its difference against the initial distribution (upper figure).

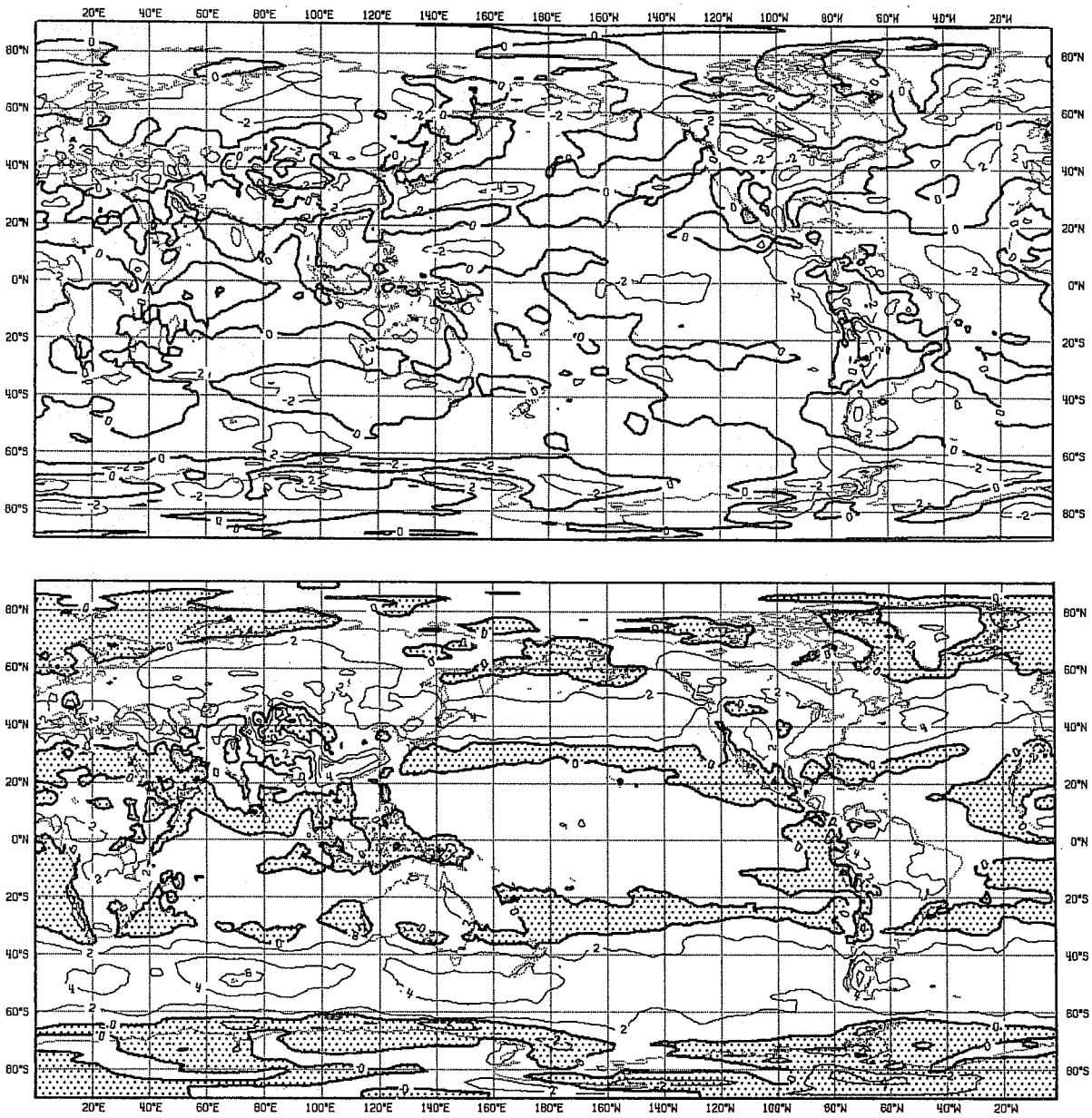

Fig. 5 Mean windshear between the top of the boundary layer (σ=0.914) and the surface layer top (σ=0.996) of all EC-forecasts for April 1981 at day 10 (lower figure) and its difference against the initial distribution (upper figure). Areas with negative shear are shaded.

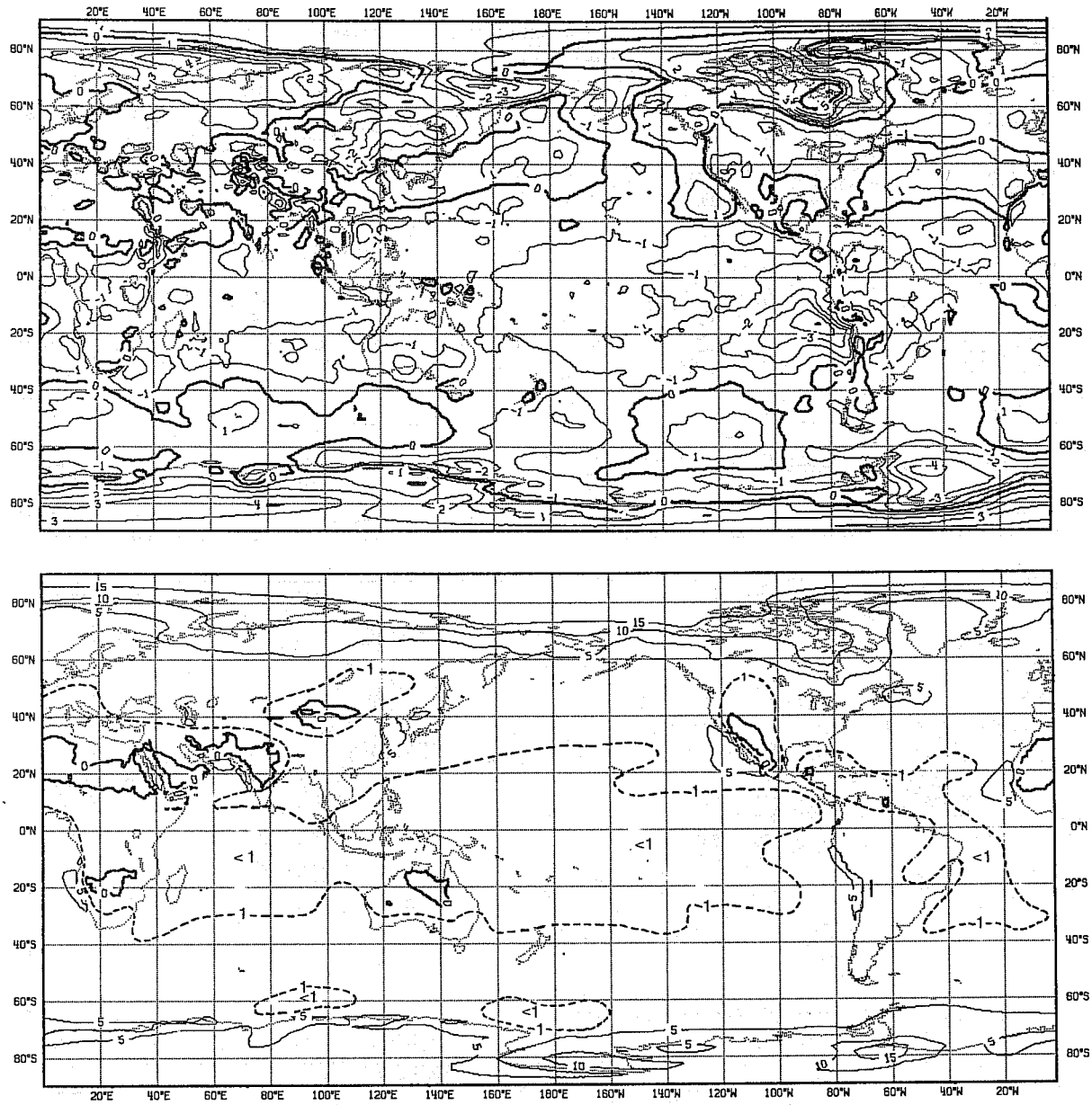

Fig. 6 Mean potential temperature difference between the top of the boundary layer (σ=0.914) and the surface layer top (σ=0.996) of all EC-forecasts for April 1981 at day 10 (lower figure) and its difference against the initial distribution (upper figure).

The total heat content of the boundary layer, which is again considered as the 3 lower model layers, decreases during the forecast in the tropical and subtropical area between 40 S and 40 N, the sensible heat content by an equivalence of 2K average and the moisture content by 2 g/kg. The heat content is unrealistically high in the initial state because cumulus convection is largely suppressed in the data assimilation. Its decrease during the forecasts is therefore justified. The thermal stability of the boundary layer is shown in Fig. 6. The boundary layer is very stable over the polar regions and also over the oceans off the west coasts of the continents over the cold upwelling water, over the East China Sea and around Newfoundland. The boundary layer is only slightly stable over the largest parts of the tropics and subtropics and is neutrally stratified over the dry subtropical regions. The geographical distribution appears altogether quite realistic.

2.2 Mean boundary layer structure for different areas

The vertical gradients of potential temperature were taken over a large depth (800m) and provide only a rough estimate of the structure of the boundary layer. The vertical structure is therefore also studied in tephigrams for several areas of an approximate size of $10^{\circ} \times 10^{\circ}$. The vertical proviles represent again the mean state for the whole month of April, 1981, as given initially and by the ensemble of all 10-day forecasts. Only a few examples are shown here.

North Africa (Fig. 7a). The boundary layer over the arid area of North Africa is determined by large surface fluxes of sensible heat ($H_s > 50$ W/m^2) and very small moisture fluxes. The boundary layer is accordingly dry convectively driven and is well mixed with regard to potential temperature and moisture (of very small amounts) over a depth of 1500 m.

Atlantic and Pacific trade wind areas (Fig. 7a and 7b). A correct simulation of the trade wind boundary layer and its processes is important as there are large amounts of heat absorbed from the ocean and transported to the tropics driving the large-scale circulation mainly through latent heat release. The structure of the trade wind boundary layer in the forecasts is, in principle, in agreement with observations, i.e. it is characterized by a well mixed moist boundary layer below a very dry atmosphere, although a well defined inversion at its top is absent in the forecasts. However, the mixed layer is apparently far too shallow, particularly over the Atlantic where its mean depth is only 200 m. The accumulated water vapour content and the amount of its downstream transport to the tropics must, therefore, be underestimated. As we will see later, the moisture supply from the ocean is indeed much smaller than in reality. Augstein et al. (1973) among others, argued that the height of the trade wind boundary layer depends on the balance of the (usually very strong) large-scale atmospheric sinking motion and the upward turbulent transports mainly by cumulus convection.

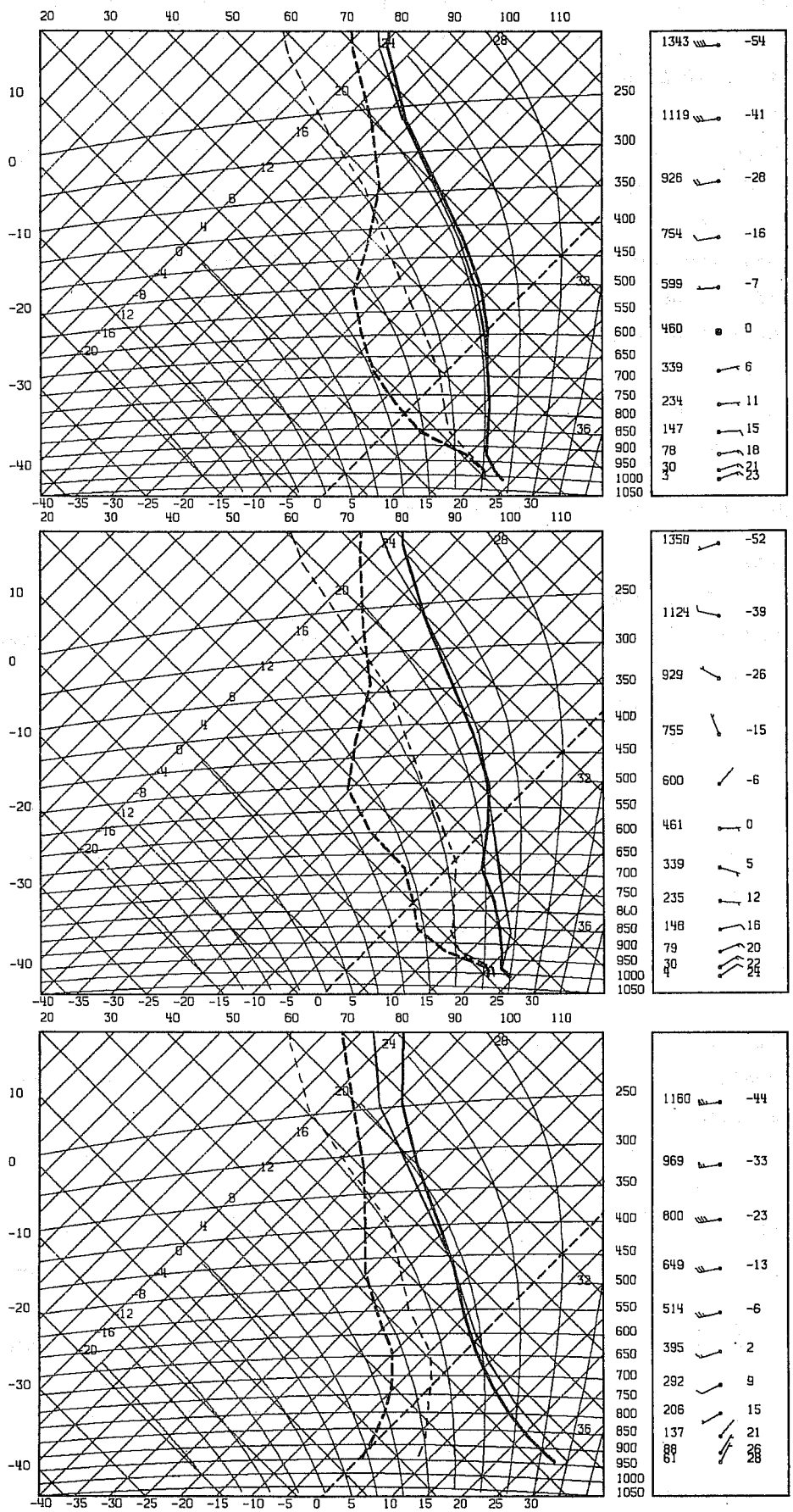

Fig. 7 Mean vertical distribution of temperature and dewpoint of all operational EC-forecasts in April 1981 at day 10 and initially (thin lines) for areas: North Africa, the Atlantic tradewinds and the Pacific tradewinds.

The most likely candidate for an imbalance in the forecasts is the underestimate of cumulus convection.

Figs. 8-10 show the mean surface fluxes of sensible and latent heat and the surface stress for the whole forecast period of 10 days.
Sensible heat flux (Fig. 8): The atmosphere receives large amounts of energy over the arid land areas in the subtropics, over the Arctic Ocean and over the Gulfstream. The sensible heat flux is downward over the polar regions, over North-America, over Siberia, along the westerlies in the Southern Hemisphere and over the Pacific. It is also downward, though small (< 12.5 W/m^2), over most of the tropical and subtropical land areas with vegetation. Over the subtropical and tropical oceans, the atmosphere receives only a small amount of energy in the form of sensible heat (< 12.5 W/m^2) which seems to agree with climatic values.

For April (S. Chart 35 in Hastenrath and Lamb, 1978), for the Atlantic and Eastern Pacific. The geographical distribution of the surface heat flux appears quite realistic and major deficiencies in the forcing of the atmospheric flow due to surface heat exchanges are not obvious from our results.

The geographical distribution of the surface latent heat flux (Fig. 9) appears also realistic. We notice large fluxes over the tropical oceans and over the Gulfstream and Kuroshio, relative minima over the oceans along the equator and very small values over North Africa and Australia. A verification is not possible, particularly not over the land. However, a comparison with climatic values calculated from observationsl data for the Atlantic and Eastern Pacific and for the Indian Ocean (see Chart 47 in Hastenrath and Lamb, 1978 and 1979) revealed systematic deficiencies in the model fluxes. Whereas the fluxes near the equator agree well with the climate values, they are underestimated over the subtropical oceans, on average by 50 W/m^2 and so over all three oceans. The existence of smaller surface fluxes agrees well with our earlier findings that the tradewind boundary layer is considerably shallower in the simulation than generally observed and we have already mentioned the implication for the moisture transport to the equator and the weakening Hadley circulation.

It was shown in the beginning that the forecasts suffered from an imbalance of the net global radiative cooling and the net global heating due to condensational processes and surface heat exchanges (Fig.1) and we concluded that the net surface energy flux is probably underestimated in the forecasts by about 20 W/m^2. From our results we may conclude that the sensible heat flux is probably realistic and that the supply of heat as latent heat is largely underestimated over the subtropical oceans. This deficiency explains the model's tendency to under-

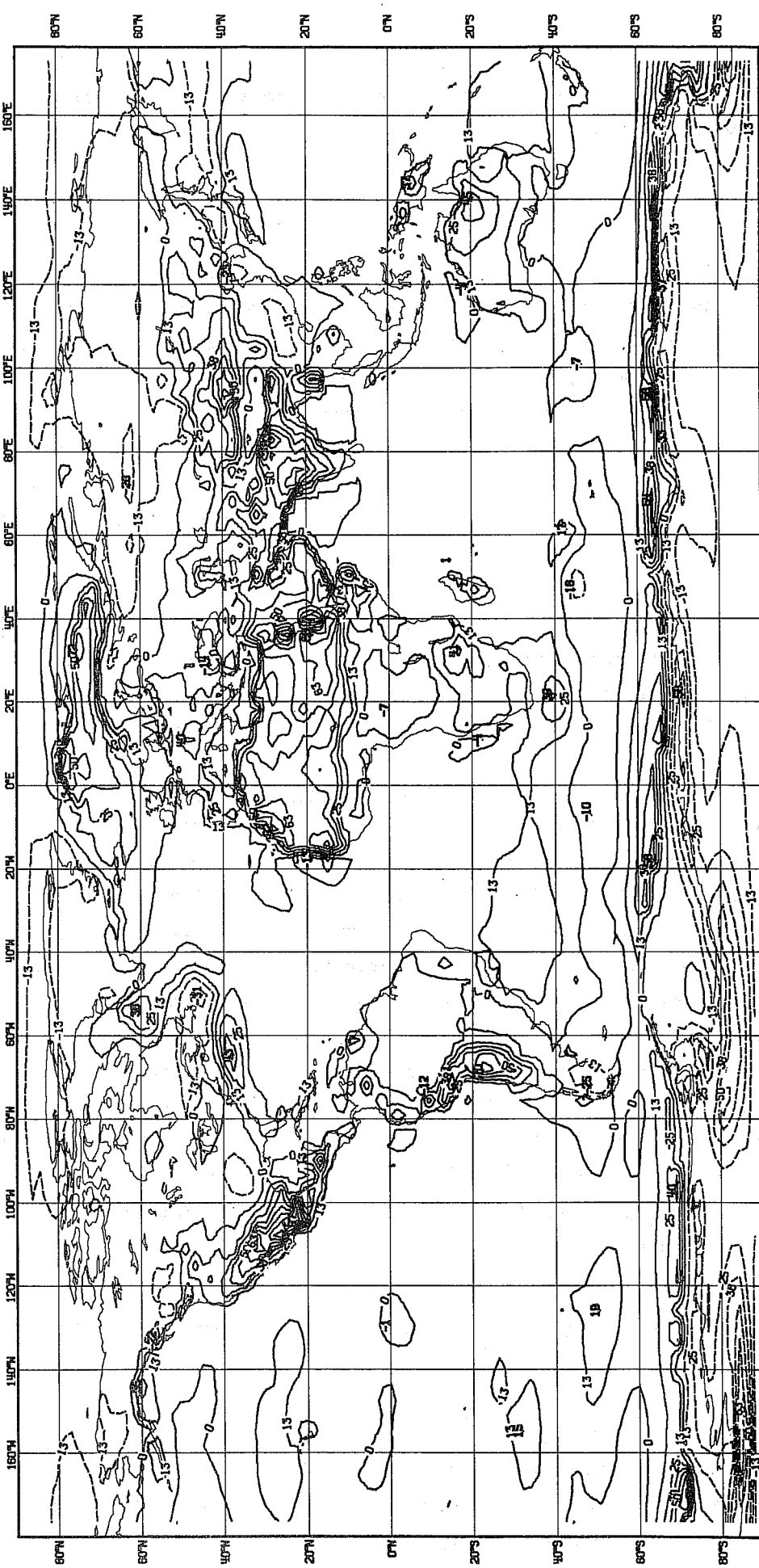

Fig. 8 Mean surface sensible heat flux (W/m^2) for all operational EC- forecasts in April 1981 for the 10 day forecast period.

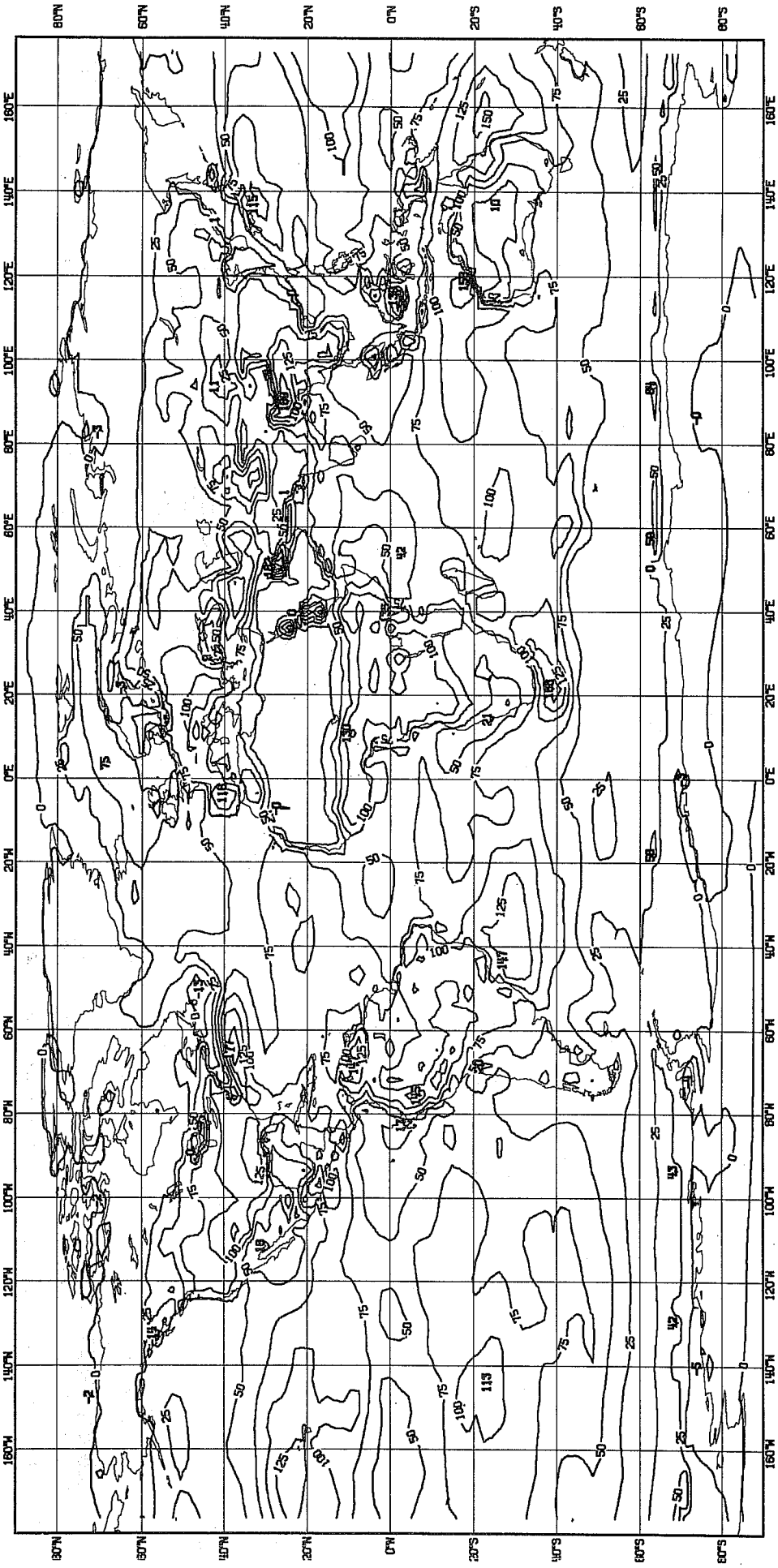

Fig. 9 As Fig. 8 except for latent heat flux (W/m^2).

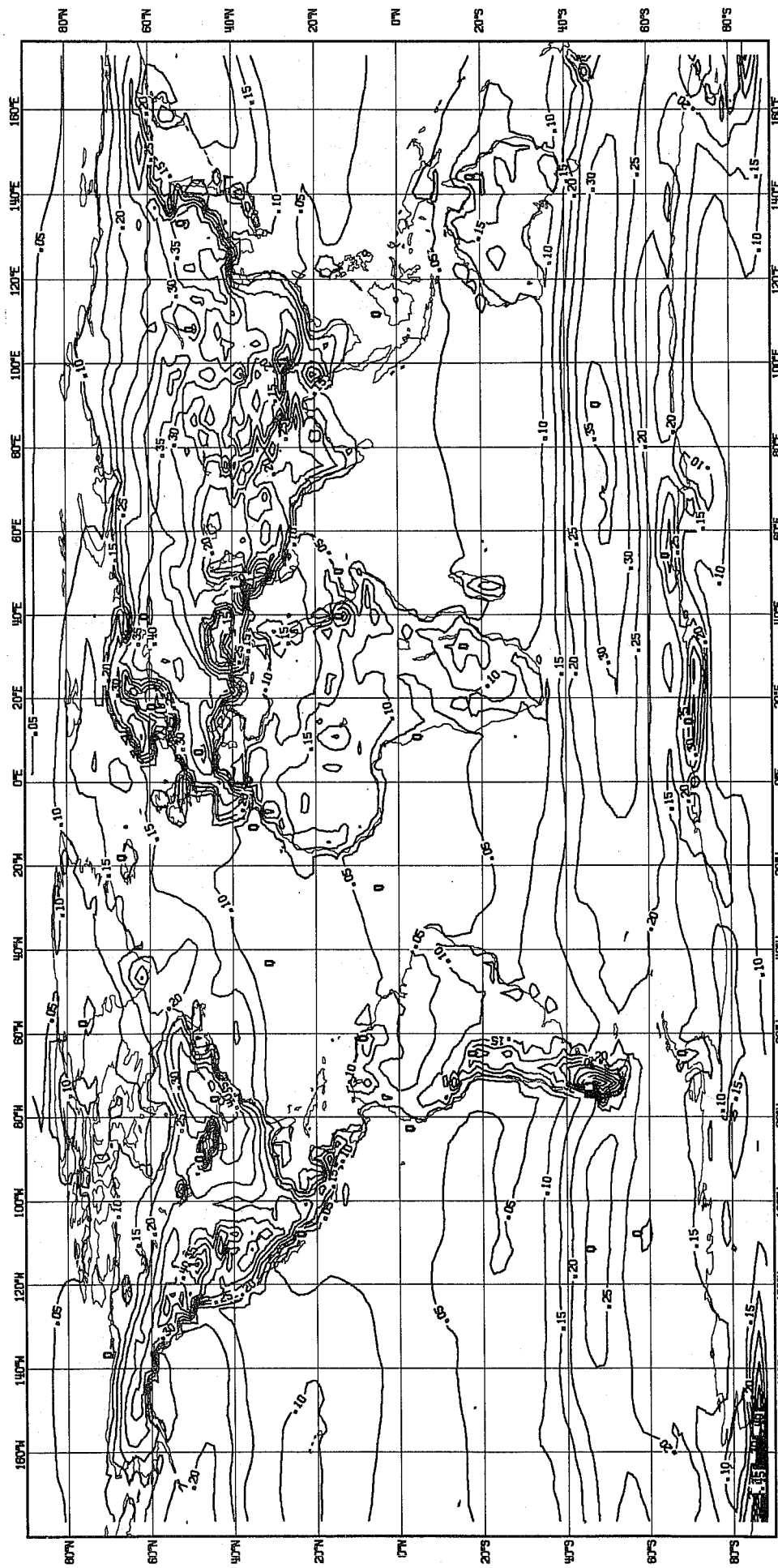

Fig. 10 As Fig. 8 except for surface stress (N/m^2).

estimate the intertropical convergence, in particular over the Atlantic.

The global distribution of the surface stress is shown in Fig. 10. Estimates of the mean surface stress over the oceans have recently been made from climate wind data (Hellerman, 1964, Han and Lee, 1981). Compared to the values given by Han and Lee (1981) for April, we find that for the ensemble of all forecasts:

(a) the surface stress is larger along the cyclone trades in the Southern Hemisphere by 0.5 N/m^2 on average exceeding 1 N/m^2 in some places.

(b) the surface stress is considerably smaller in the trade wind areas. In the NE tradewind area the surface stress is less than half the estimated climate values.

In summary, the assessment of the mean boundary flow shows:

The mean boundary layer flow and the associated surface exchanged of momentum and heat appear realistic in most areas.

Large deviations from the observed mean flow are observed over the tradewind areas where a large deficit in the moisture supply from the sea was found and along the cyclone trades in the Southern Hemisphere, where the mean boundary layer flow is too intense and leads to excessive surface friction.

2.3 Case studies

From the assessment of the mean boundary layer flow it is not possible to judge the quality of the parameterization of the boundary layer processes, as the mean flow evolves as a result of the turbulent processes and the external forcing (pressure gradient, baroclinicity, etc.). In particular, the intensification of the mid-latitudinal boundary layer flow may not necessarily be due to erroneous parameterization of turbulent processes but can similarly result from overdevelopment of baroclinic disturbances for different reasons. A reliable verification of the parameterization of boundary layer processes, and its effect on the mean flow, can, however, be obtained by case studies, where all processes but the turbulent processes are well prescribed. Three case studies are presented here:

(1) Air mass transformation in the mid-latitude.

(2) Warm sector of a cyclone (Leipzig Profile).

(3) Deep convection (GATE).

Case 1: Cold air outbreak over East China Sea (18.1.79)

A case of a polar outbreak over the East Pacific was chosen from the FGGE observing period (18.1.79) and a numerical forecast was made with the Centre's operational forecast model where the Kuo convection scheme was replaced by the convection scheme designed by Arakawa and Schubert (1974). The initial flow is shown in Fig. 11 together with the surface temperature field. Cold and dry continental air is advected over the relative warm sea. As the strong north-westerly flow prevailed for 1 day and was well predicted, this case appeared suitable for verifying the parameterization of turbulent and convective processes in the EC-model. The continental air is heated and moistened from below when advected over the sea. The geographical distribution of the surface fluxes of sensible and latent heat (Fig. 12) agress qualitatively with that given by Ninomiya (1977) for this region. The surface heat flux is largest over the Japan Sea (widespread above 300 W/m^2) and in msot parts exceeds the latent heat flux. Consequently, a Bowen ratio larger than 1 was found in agreement with Ninomiya (1977). Over the East China Sea the surface fluxes of heat and moisture increase downstream towards the Kuroshio region. The latent heat flux exceeds 600 W/m^2 south of Kyushu and is twice the sensible heat flux. The Bowen ratio of 0.5 also agrees well with that estimated by Ninomiya (1977) for this region. The largest precipitation rates were predicted over the Pacific east of the Kuroshio region and is located further to the east and to the north than observed for the period of strong cold air outbreak during AMTEX 74 (Ninomiya and Akiyama, 1976). The lack of precipitation over the East China Sea on the other hand agrees well with observations for the same period (Ninomiya and Akiyama, 1976).

A detailed budget calculation for the 1-day forecast period was made for the model's grid point nearest to NAZE on a Southwest Island east of the China Sea, where upper air soundings are available for this period. Predicted and observed vertical soundings of temperature, moisture and wind are shown in Fig. 13. The overall agreement is good. Temperatures differ by less than 2K in the lower boundary layer, but there are significant differences with respect to the height of the inversion and with respect to the moisture content below the inversion. The inversion appears lowered by 50 mb in the forecast and the air is much drier under the inversion. The existence of an almost saturated layer and a corresponding cloud layer under the inversion was also confirmed during the AMTEX period (Ninomiya and Akimaya, 1976). Except for these differences the

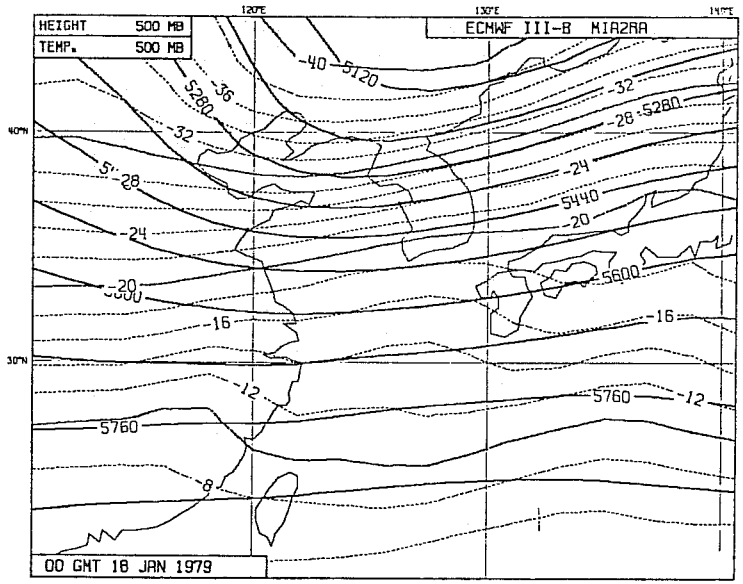

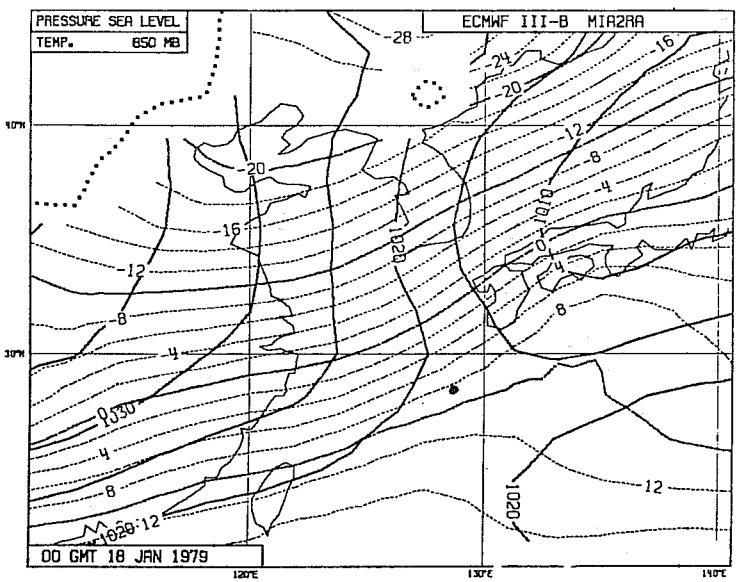

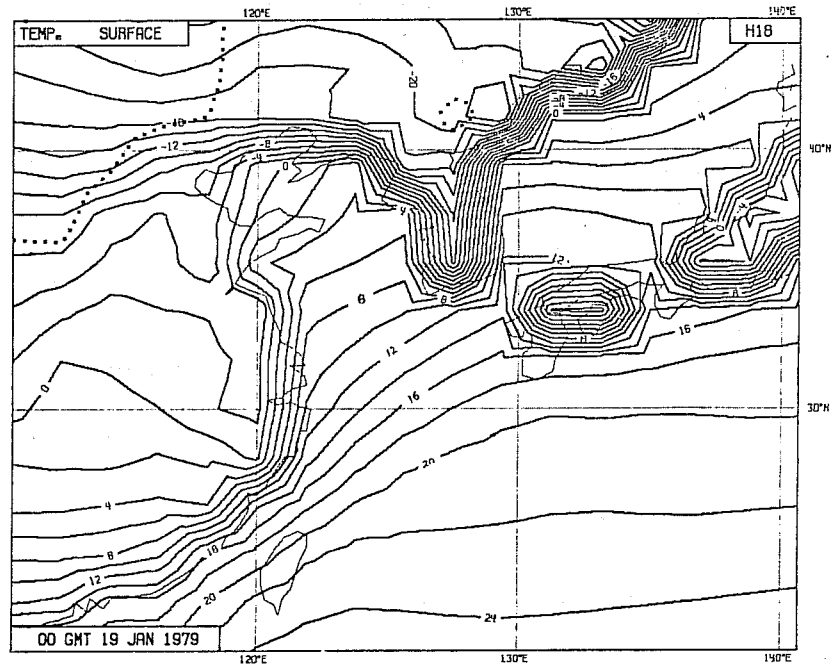

Fig. 11 Initial distribution of H_{500}, T_{500}, P_s and T_{850} at 00 GMT 18 January 1979 (ECMWF-FGGE) and surface temperature distribution.

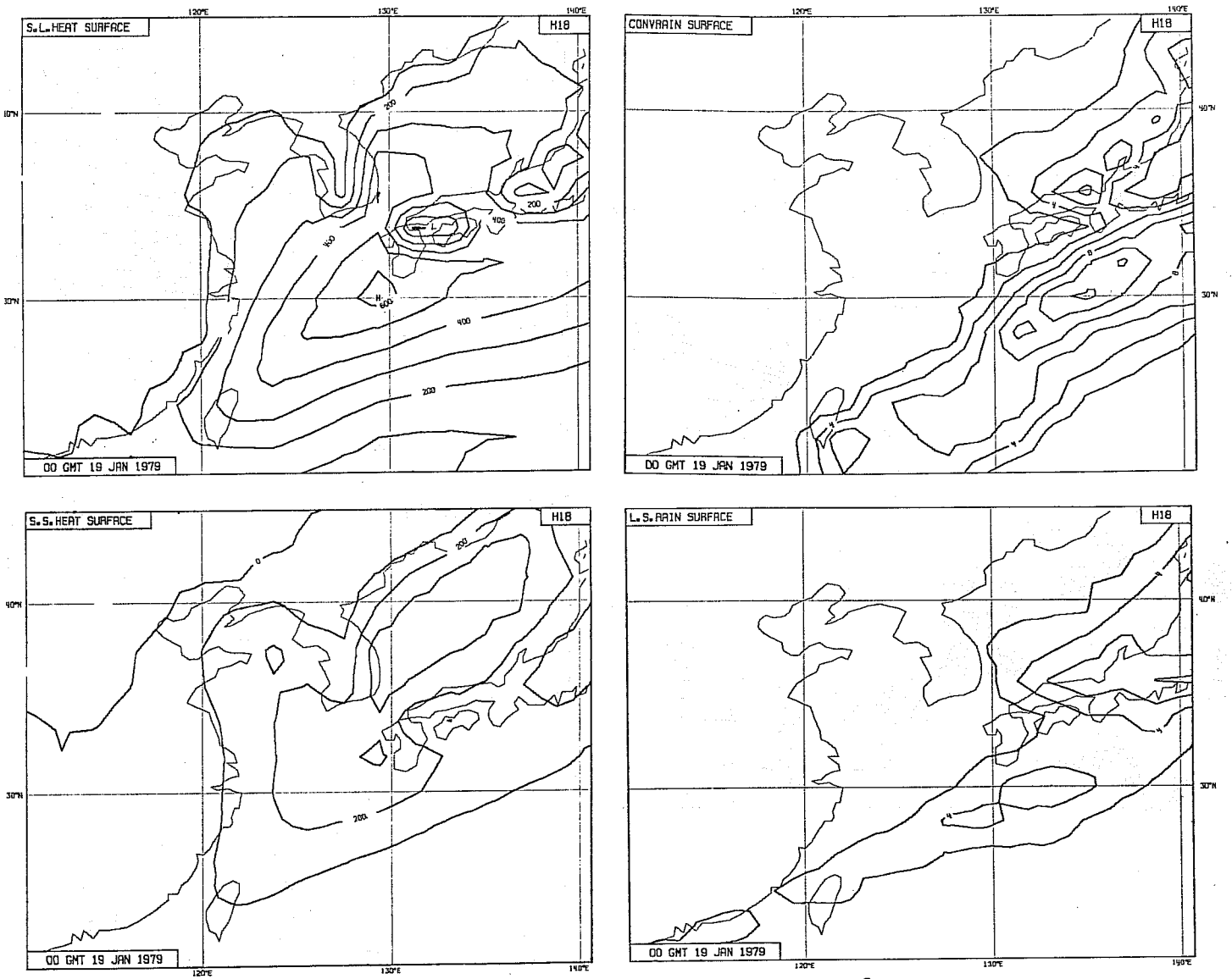

Fig. 12 Distribution of the mean surface fluxes of sensible and latent heat (W/m^2) and of the convective and large-scale precipitation (mm/day) during the first day of the forecast.

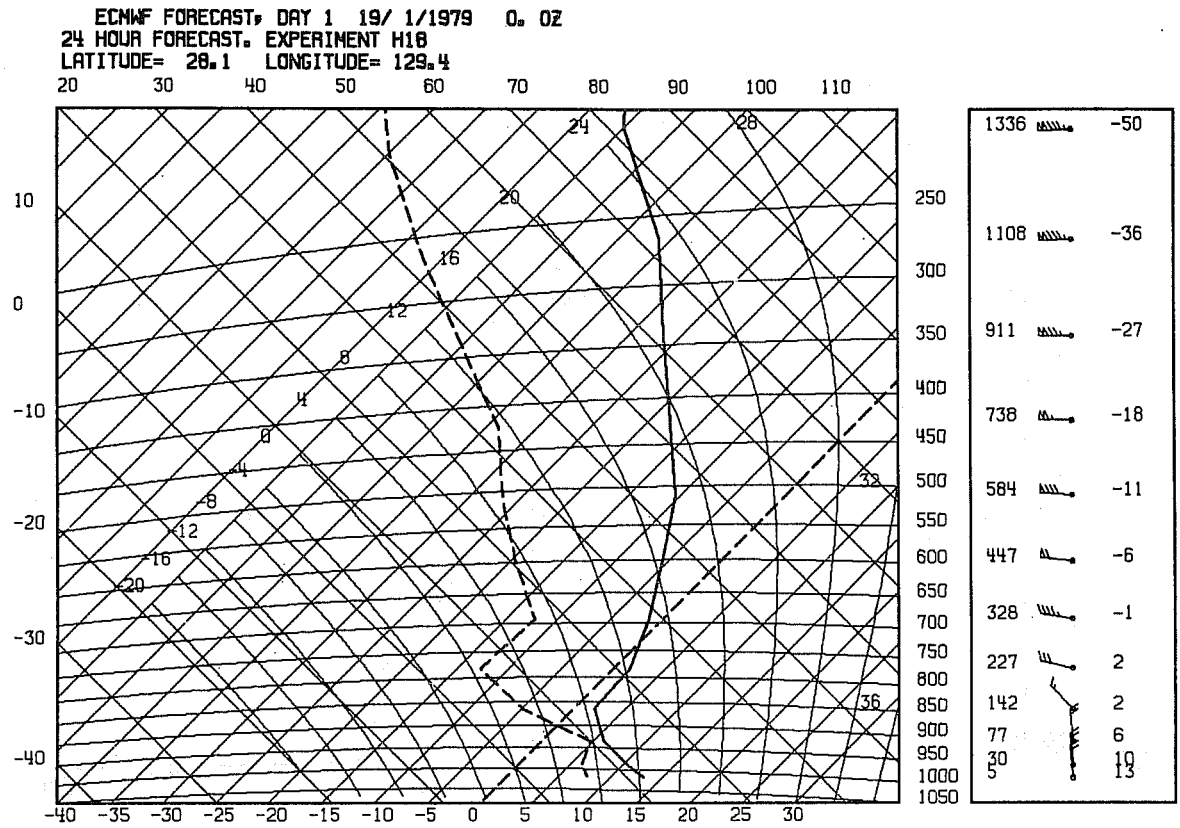

FGGE OBJASA

47909 28N 129E 0 GMT 19 JAN 79

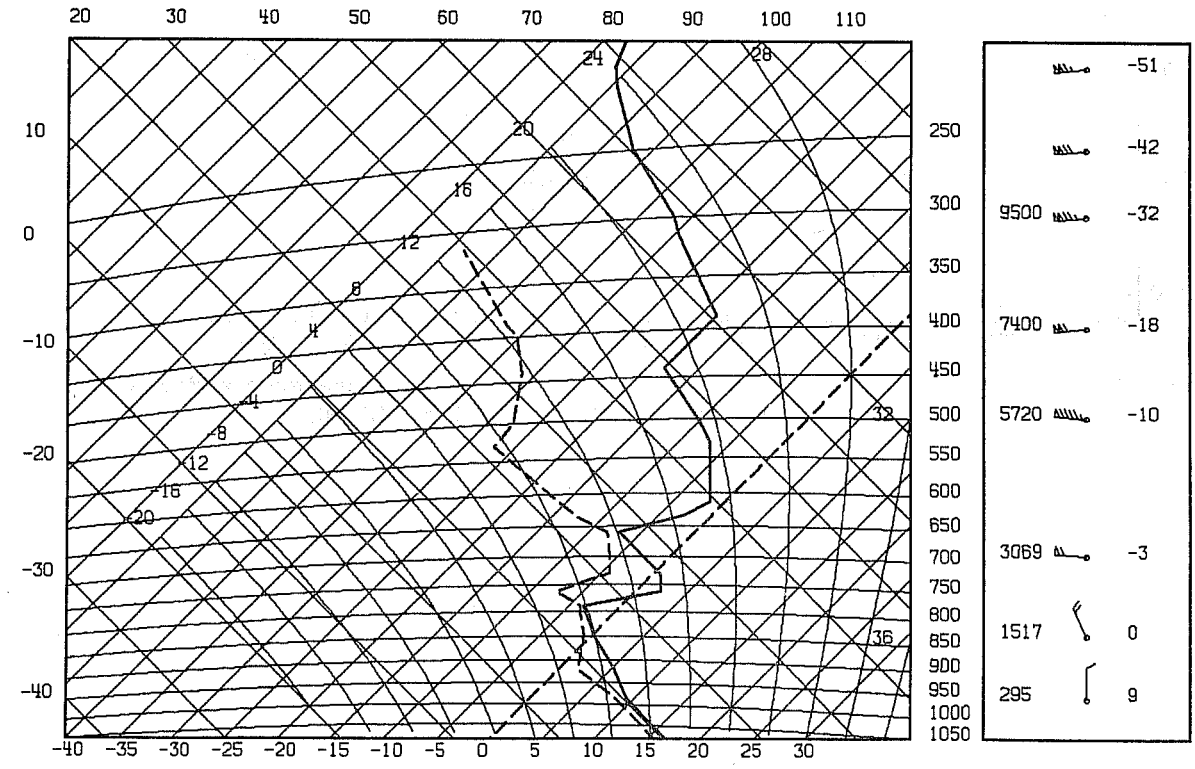

Fig. 13 Vertical distribution of temperature and dewpoint at 00 GMT 19 January 1979 (lower figure) observed at NAZE; (upper figure) predicted at the nearest gridpoint.

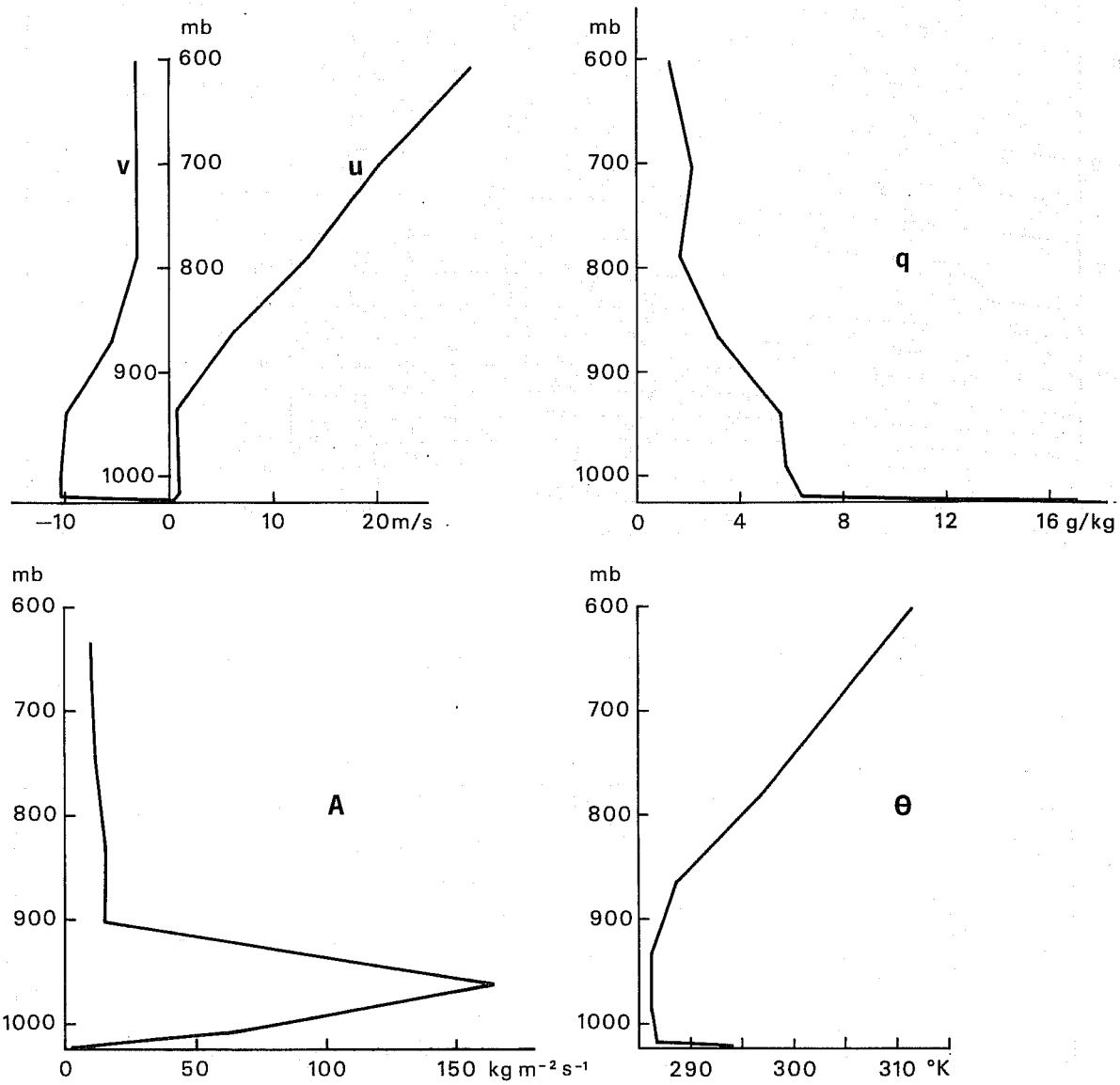

Fig. 14 Vertical distribution of u,v,θ and of the heat exchange-coefficient A in the forecast after 1 day at gridpoint (28.1°N, 129°E).

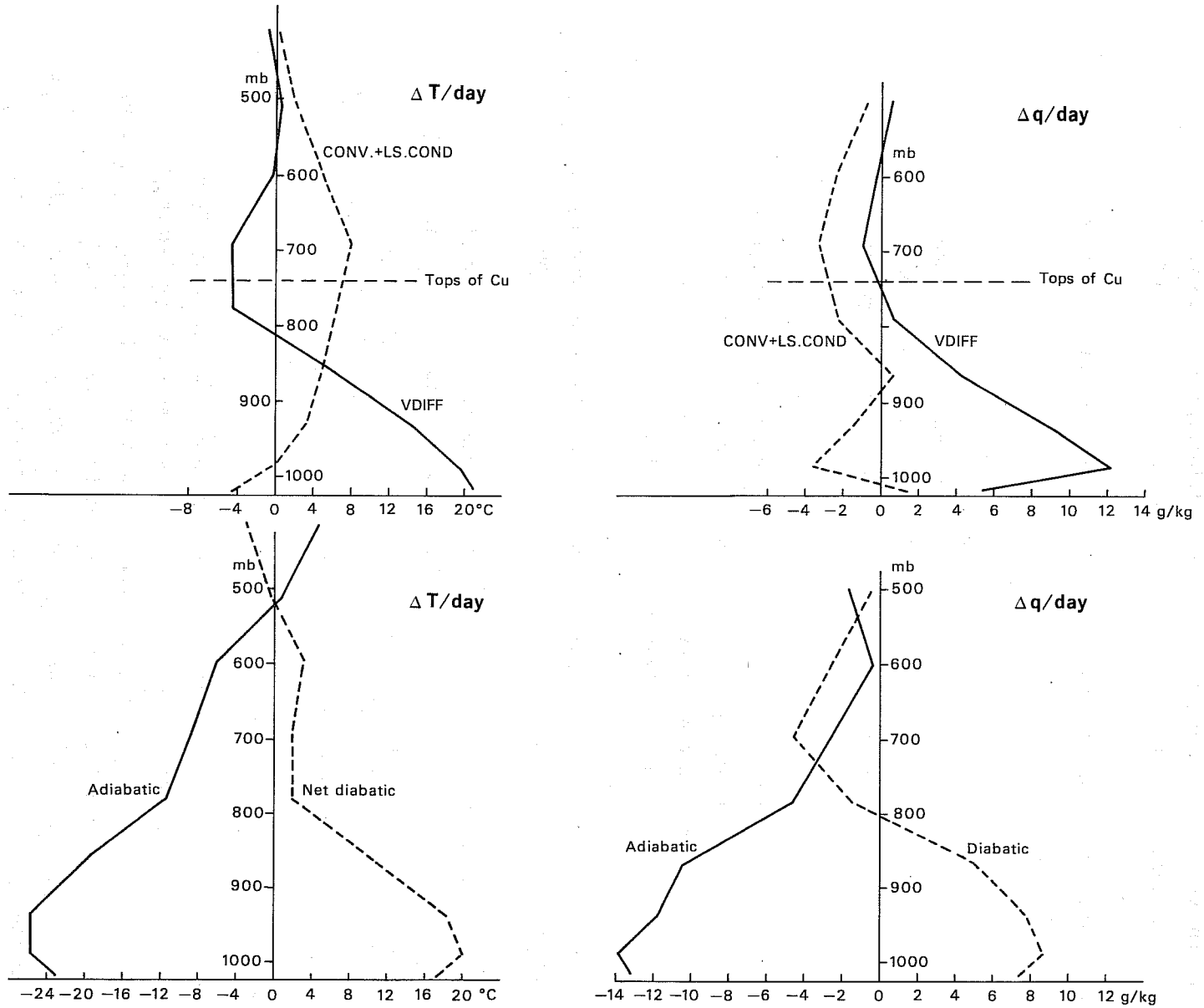

Fig. 15 Vertical distribution of the one day averaged heating and moistening rates in the forecast at gridpoint (28.1°N, 129°E).

vertical structure of temperature, moisture and momentum appear very realistic in the forecast (Fig. 14). The lapse rate is superadiabatic near the surface, adiabatic above up to 930 mb and then moist-adiabatic up to 850 mb. Moisture and momentum are also well mixed in the boundary layer below 950 mb except for the surface layer in agreement with AMTEX (Ninomiya and Akimaya, 1976). The budget calculated at the same gridpoint for the one-day period shows (Fig.15):

(1) The large local cooling and drying due to adiabatic processes (mainly by horizontal advection of cold and dry air) is largely compensated by diabatic heating and moistening.

(2) The atmosphere is heated at lower levels mainly by vertical fluxes of sensible heat, around 850 mb by convection and higher up by latent heat release associated with large-scale rising motion.

(3) The lower troposphere up to 700 mb is moistened by vertical fluxes of water vapour and to a smaller degree dried out by convection and condensation processing, except at 850 mb and near the surface (evaporation of rain).

The vertical profiles of heating and moistening within the boundary layer agree well with those presented by Ninomiya and Akimaya (1976) for AMTEX.

Summarizing, we may say that the rapid transformation of the cold and dry polar air is well simulated by the parameterized diabatic processes in the EC-model. Deficiencies are found with respect to the location and the character of the inversion which is lower down in the atmosphere than observed and which is not connected with a cloud layer as observed.

Case 2: The Leipzig Profile

As cyclones, particularly in their decaying stage, are strongly affected by internal friction and by the surface stress besides other processes, the boundary layer flow and its parameterized processes, like internal friction, ought to be verified in relevant cases. Unfortunately, a suitable case study from the period of operational forecasts at ECMWF was not prepared in time for this workshop. Instead, the classical "Leipzig wind profile" (Mildner, 1931) was chosen, which describes in detail the vertical wind distribution in the slightly stable warm air of a well developed cyclone. As the flow was strong and steady and also uniform due to the absence of convection, this wind profile is considered as a unique example of the representative wind distribution in the boundary layer. Our study consists of a simulation experiment to investigate

the steady state flow which would develop if all processes were prescribed but turbulent fluxes of momentum and the effect of the earth's rotation on the flow. The model used is a single column version of the global model where the flow is fully determined by the horizontal momentum equation only:

$$\frac{\partial V}{\partial t} = fk \times (Vg-W) - g \frac{\partial \bar{u}}{\partial p}$$

the turbulent fluxes of momentum π depend on the windshear and on the thermal stability in the same way as in the full model. The initial flow is the wind profile re-examined by Lettan (1950), the geostrophic wind (v_g = 15 m/sec) and the lapse rate ($\partial T/\partial z$ = 0.65K/100 m) are uniform throughout the boundary layer. Surface temperature (T_s = 291.5K) and surface roughness (Z_o = 0.07m) are specified following Carson (1976). The result of the simulation is summarized in Fig. 16-18. The adjustment to a steady state was quick as is for example seen from the time evolution of the surface stress (Fig. 17), which does not alter after 12 hours. The simulated steady state wind profile (Fig. 16) agrees well with the observed profile in the upper part of the boundary layer, but differs considerably in its lower part, where the simulated flow is stronger, at the lowest level (730 m) by approximately 2-3 m/sec. In spite of the increased surface wind, the surface stress (Fig. 17) is still slightly smaller in the simulation (0.50 N/m^2 compared to Lettan's value of 0.53 N/m^2). This comparable small surface stress is, however, consistent with the momentum exchange coefficients (Fig. 18) which are much smaller than those calculated by Lettan (1950) and also by Carson (1976). Various reasons can account for these differences like unrealistic momentum exchange coefficients in dependence on thermal stability, vertical truncation errors due to coarse vertical resolution of the boundary layer or even the assumption of steady state or the neglect of nonlinear processes. Sensivity tests are therefore performed to investigate the effect of the surface roughness and the thermal stability on the turbulent momentum exchange and thereby on the simulated flow. It was found that the steady state flow is rather insensitive to small changes in the thermal stability (changed from 0.65^o/100 m to 0.75^o/100 m) and in the surface roughness length Z_o. Only a drastic change of Z_o from 7cm to 70cm significantly altered the flow and the surface stress as the wind in the direction of the geostrophic wind decreased by 2m/sec, although the cross isobar flow remained nearly unchanged. The value of 70cm is very close to the value which is presently used in the global forecast model for this region.

In summary, we may conclude that the present parameterization scheme probably underestimates the turbulent momentum exchange in near neutral conditions and therefore favours strong surface winds. However, the resulting surface stress

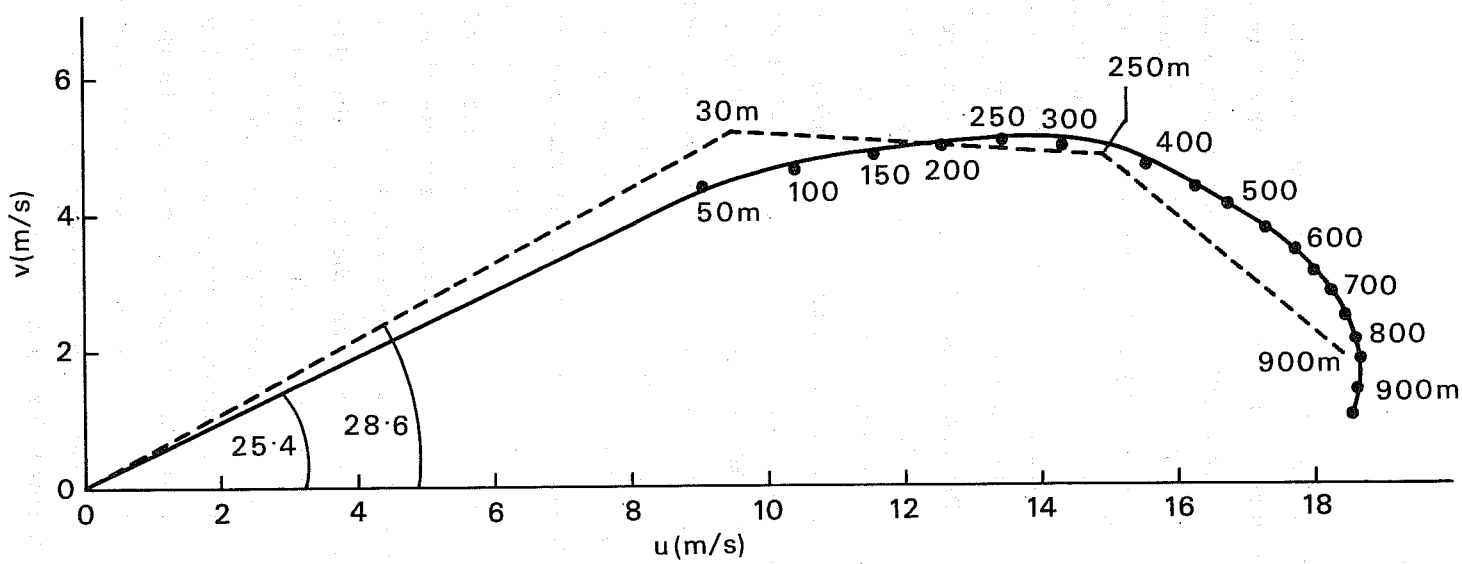

Fig. 16 Simulated and observed Leipzig wind profile (lettau (1950)).

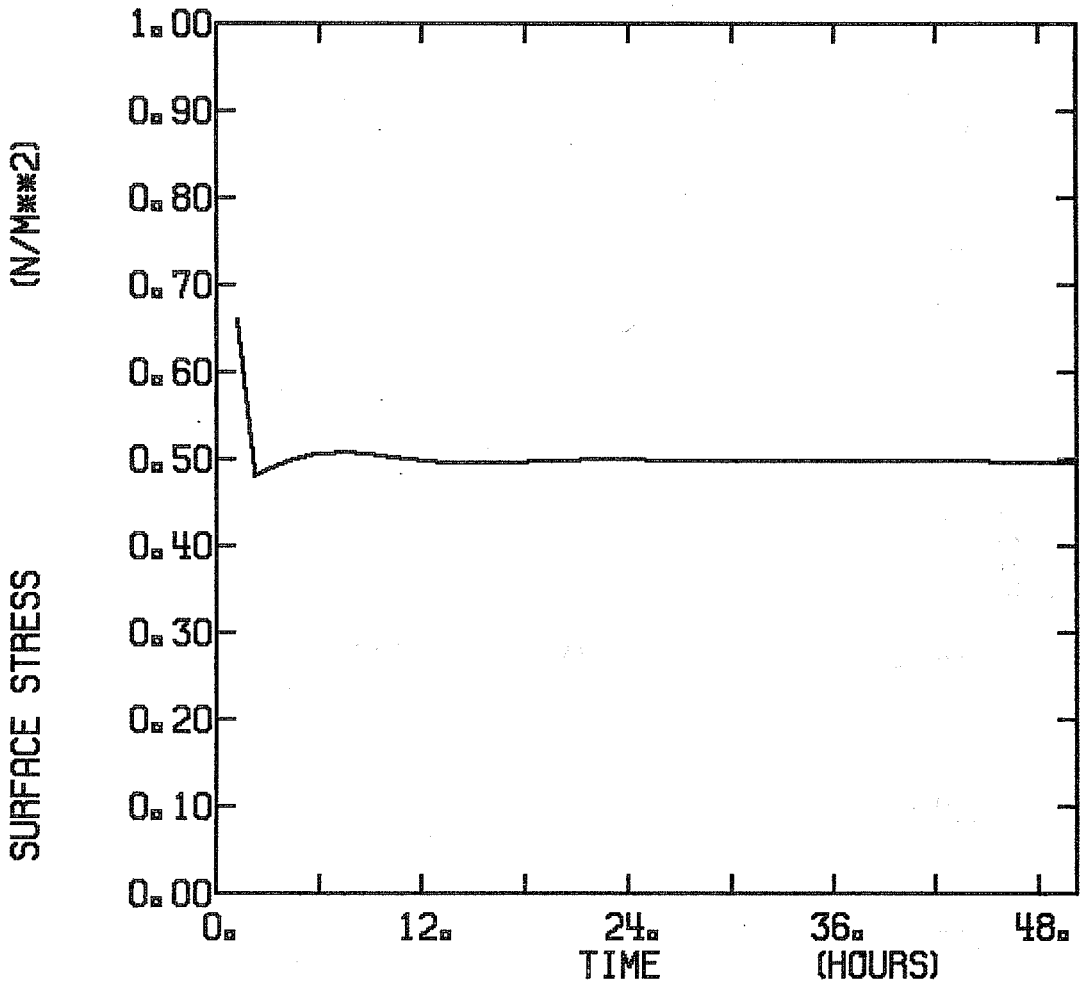

Fig. 17 Time evolution of surface stress in the simulation of the Leipzig wind profile.

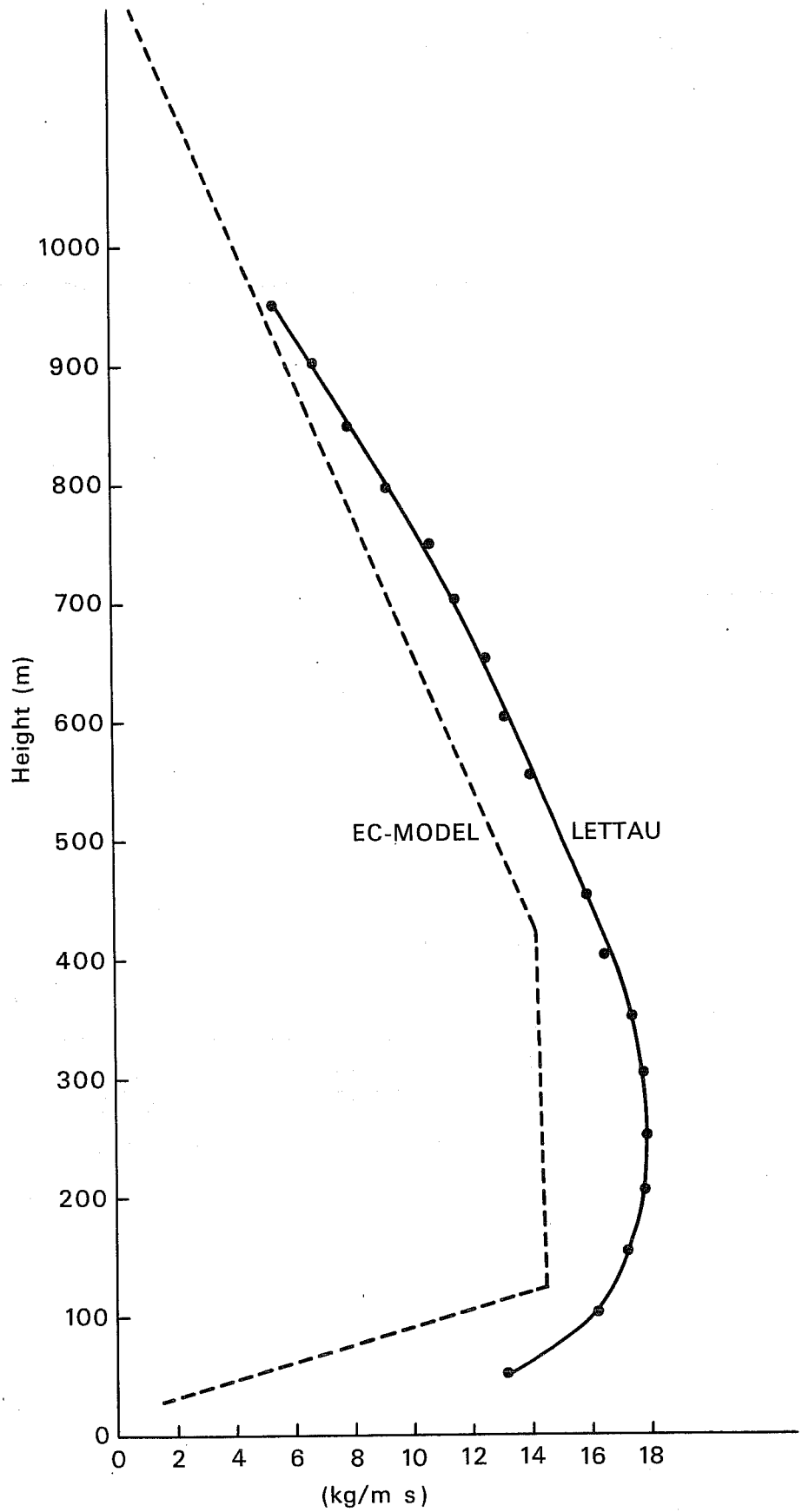

Fig. 18 Vertical distribution of the momentum exchange coefficients
a) from the observed profile derived values (Lettau (1950))
b) values in the simulation.

may still be realistic. Further experiments are,however, needed to confirm this conclusion and to clarify also the effect of vertical discretisation of the boundary layer on the simulated flow.

Case 3: GATE (boundary layer under deep convection)

In the last case study we consider the boundary layer under deep convection. The case chosen is the easterly wave composited from the data of Phase III of GATE by Reed (S. Thompson et al., 1979). Again, all processes but turbulent and convective processes are prescribed in time and a single column model is therefore used. As we are only concerned with the thermodynamical aspect of the boundary layer, the windfield is also specified. The model equations reduce therefore to the equations for temperature T and moisture q:

$$\frac{\partial T}{\partial t} = A_T + Q_r - \frac{g}{c_p}\frac{\partial F}{\partial p} + \left(\frac{\partial T}{\partial t}\right)_{cu}$$

$$\frac{\partial q}{\partial t} = A_q - \frac{g}{c_p}\frac{\partial E}{\partial p} + \left(\frac{\partial q}{\partial t}\right)_{cu}$$

where A_T and A_q are the prescribed temperature and moisture tendencies due to advection, Q_r is the prescribed radiative heating rate, F and E are the turbulent fluxes of sensible heat and moisture, respectively, and $(\partial T/\partial t)_{cu}$ and $(\partial q/\partial t)_{cu}$ are the contributions from convection. Convection is parameterized by means of the Arakawa-Schubert scheme, which performed much better in this case than the "operational" Kuo-scheme.

The initial data are those for wave category 1 and the integrations are extended for the period of a passage of one easterly wave, i.e. over all 8 wave categories (forecast period ~ 80 hrs).

Three experiments are described here which vary with respect to the processes being parameterized.

Exp. 1 : Parameterization of turbulent fluxes and convection.

Exp. 2 : Parameterization of convection only.

Exp. 3 : Parameterization of turbulent fluxes only.

In experiment 2 the surface fluxes of heat and moisture are prescribed in time and it is assumed that they decrease linearly with height up to the base of the

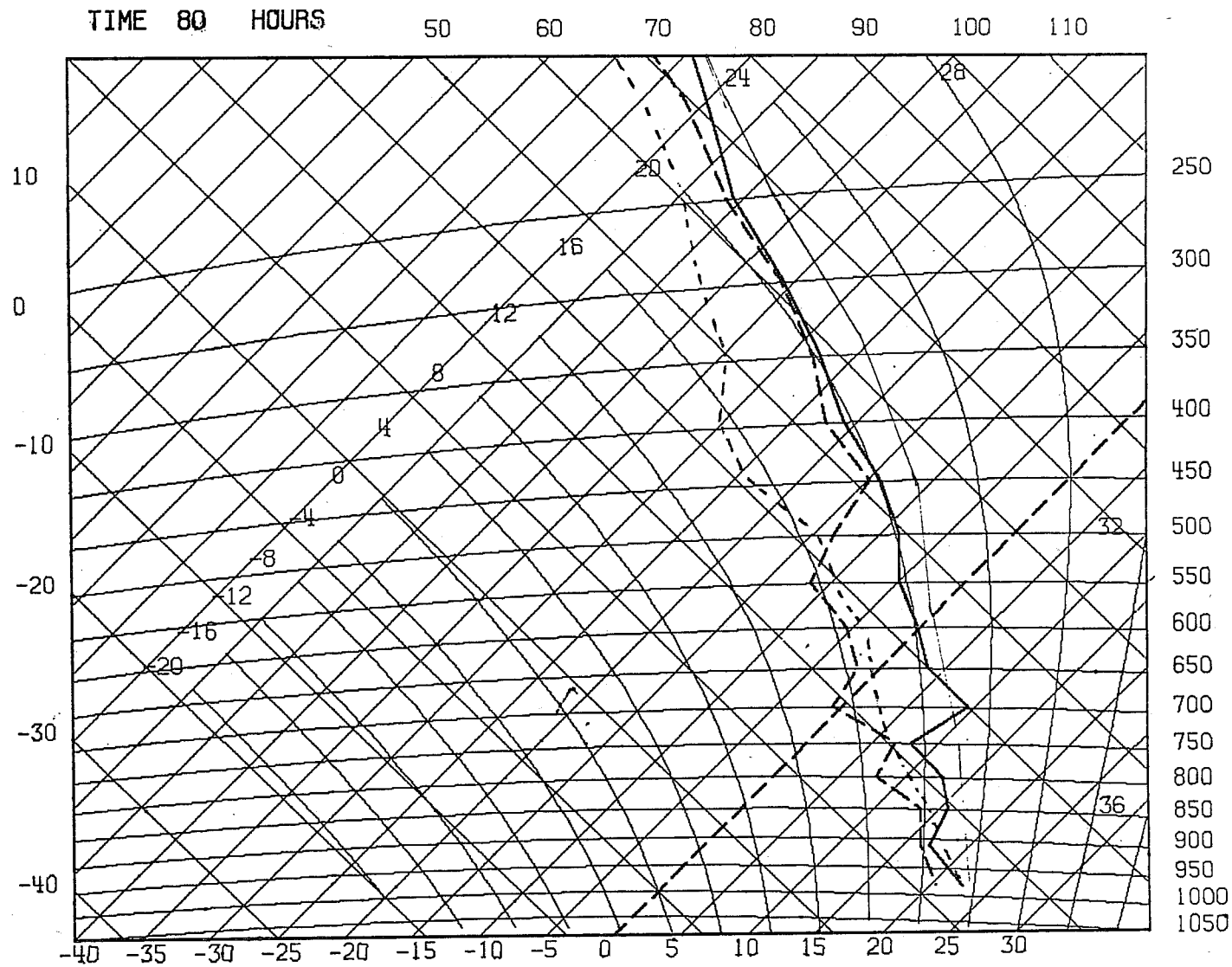

Fig. 19 Vertical distribution of temperature and dewpoint for GATE composite wave simulation experiment 1;
a) predicted distribution after 80 h (thick lines)
b) observed distribution for wavecatagory 1 (thin lines).

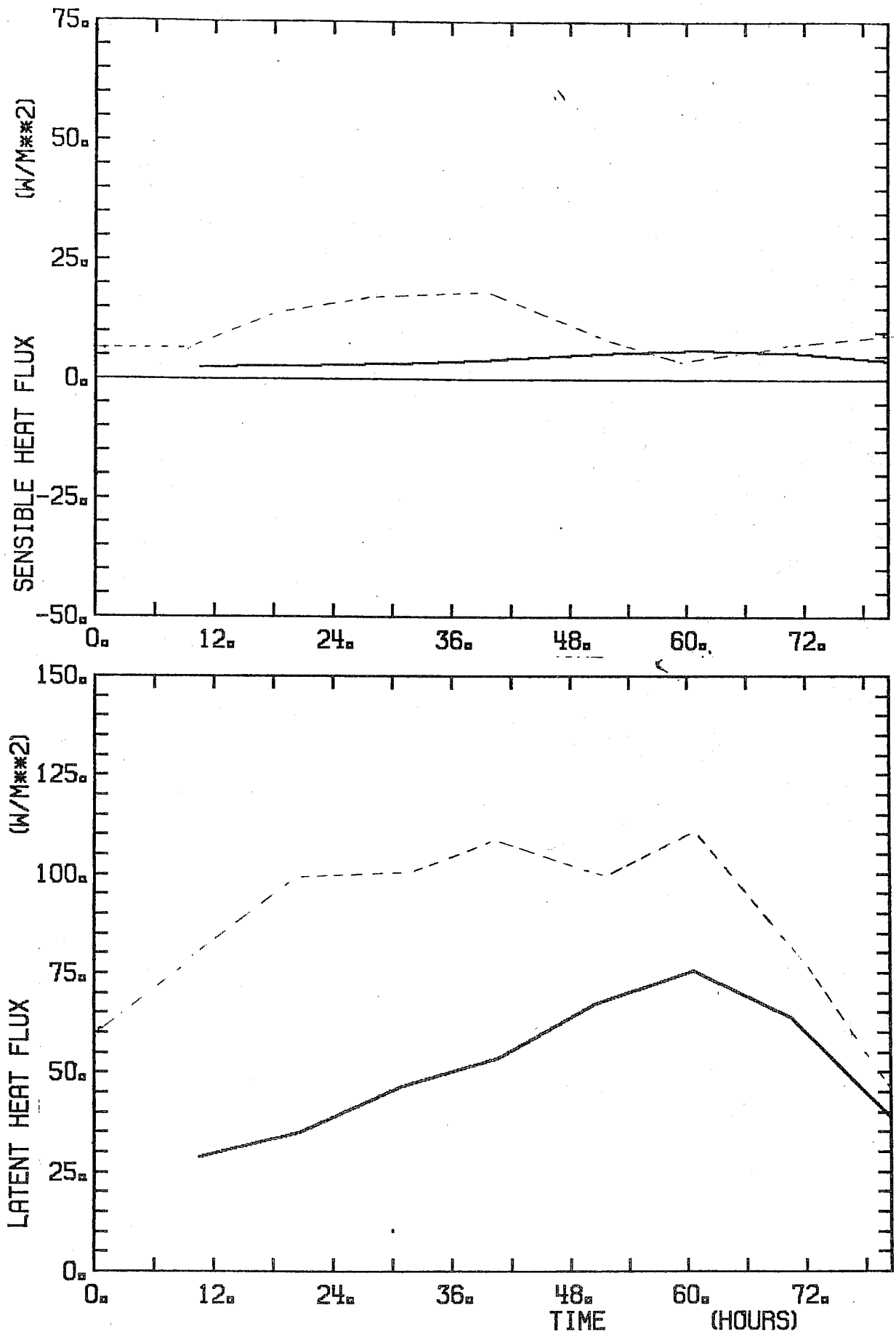

Fig. 20 Time evolution of surface fluxes of sensible and latent heat in GATE experiment 1 (observed values are dashed).

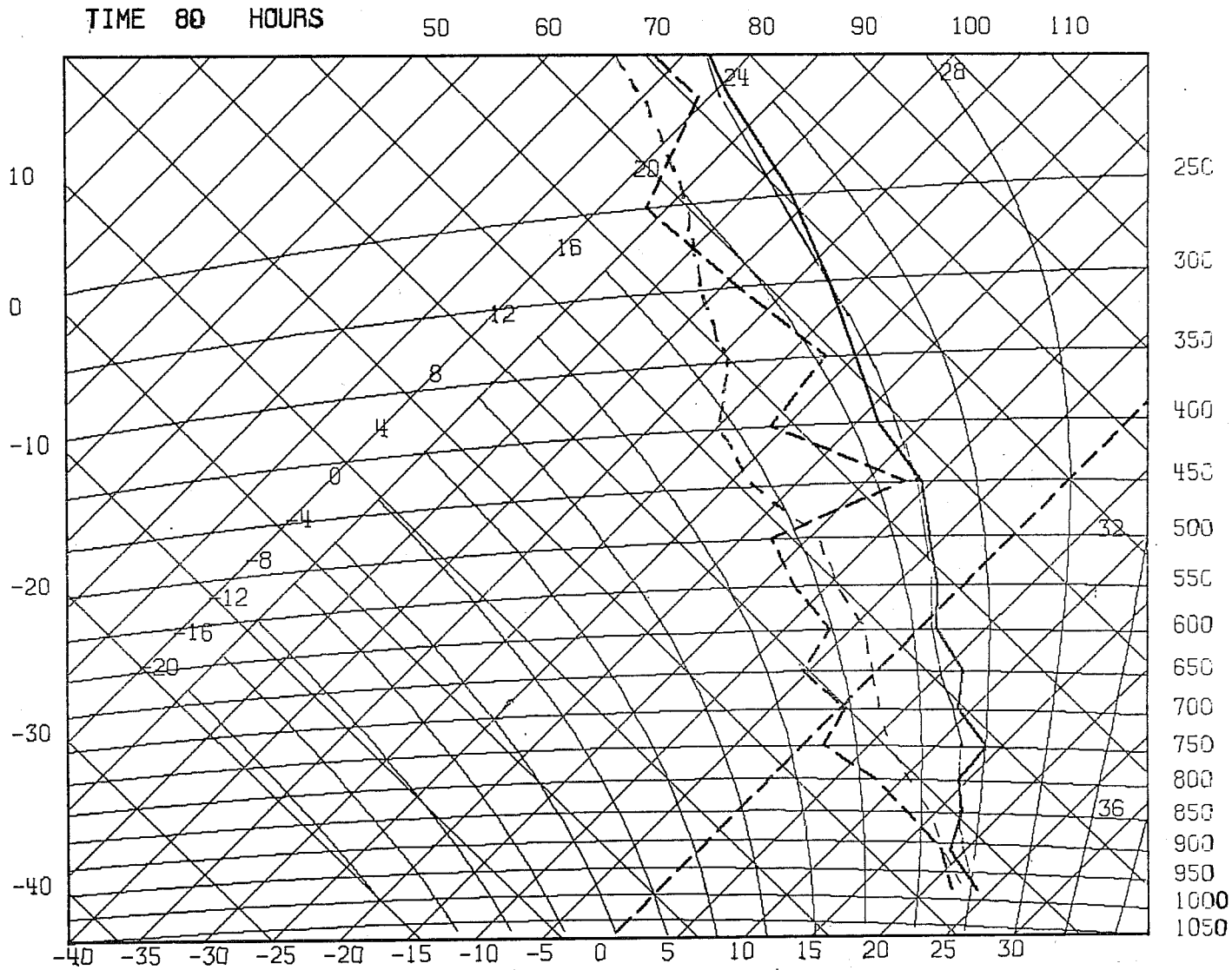

Fig. 21 As Fig. 19 except for experiment 2.

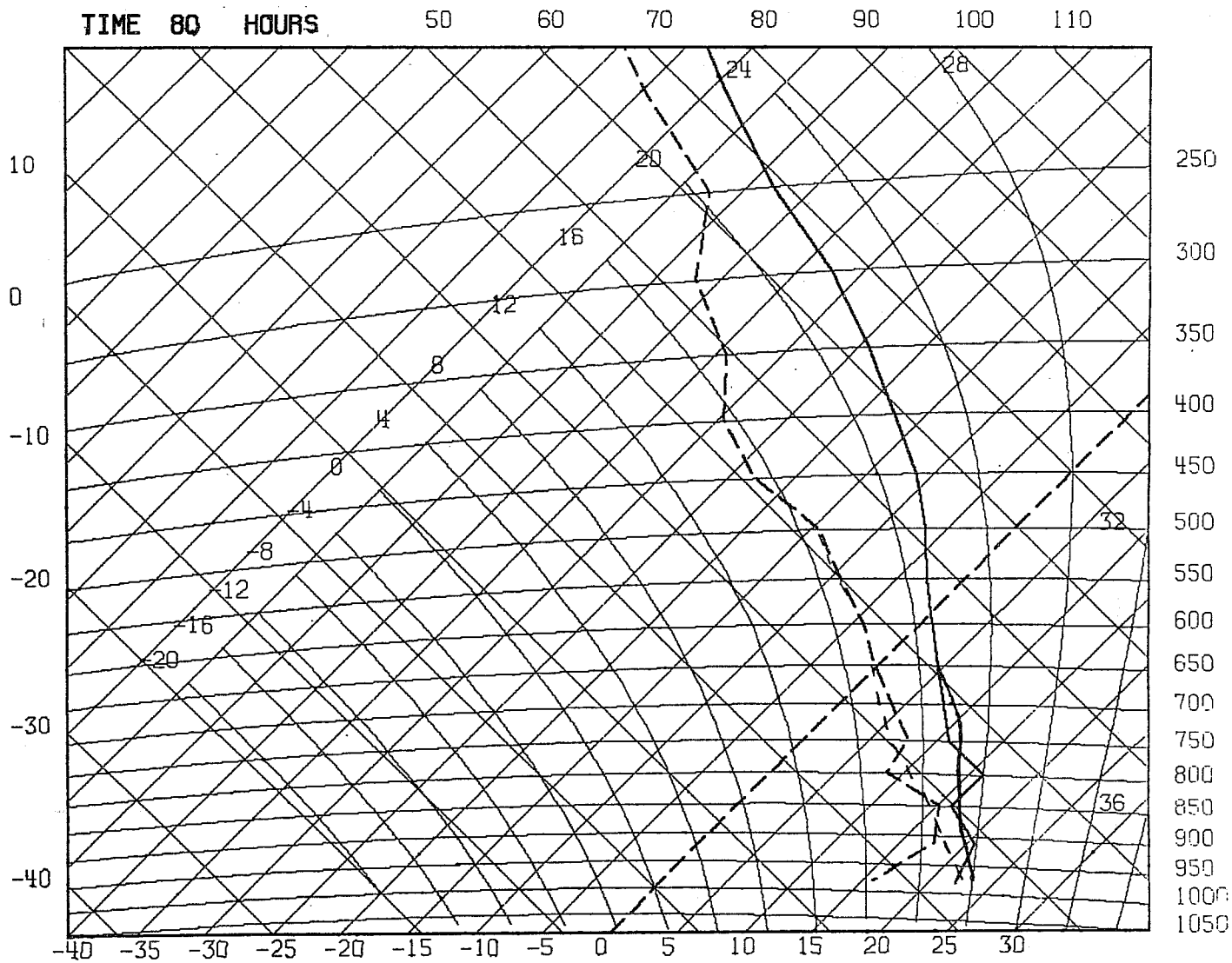

Fig. 22 As Fig. 19 except for experiment 3.

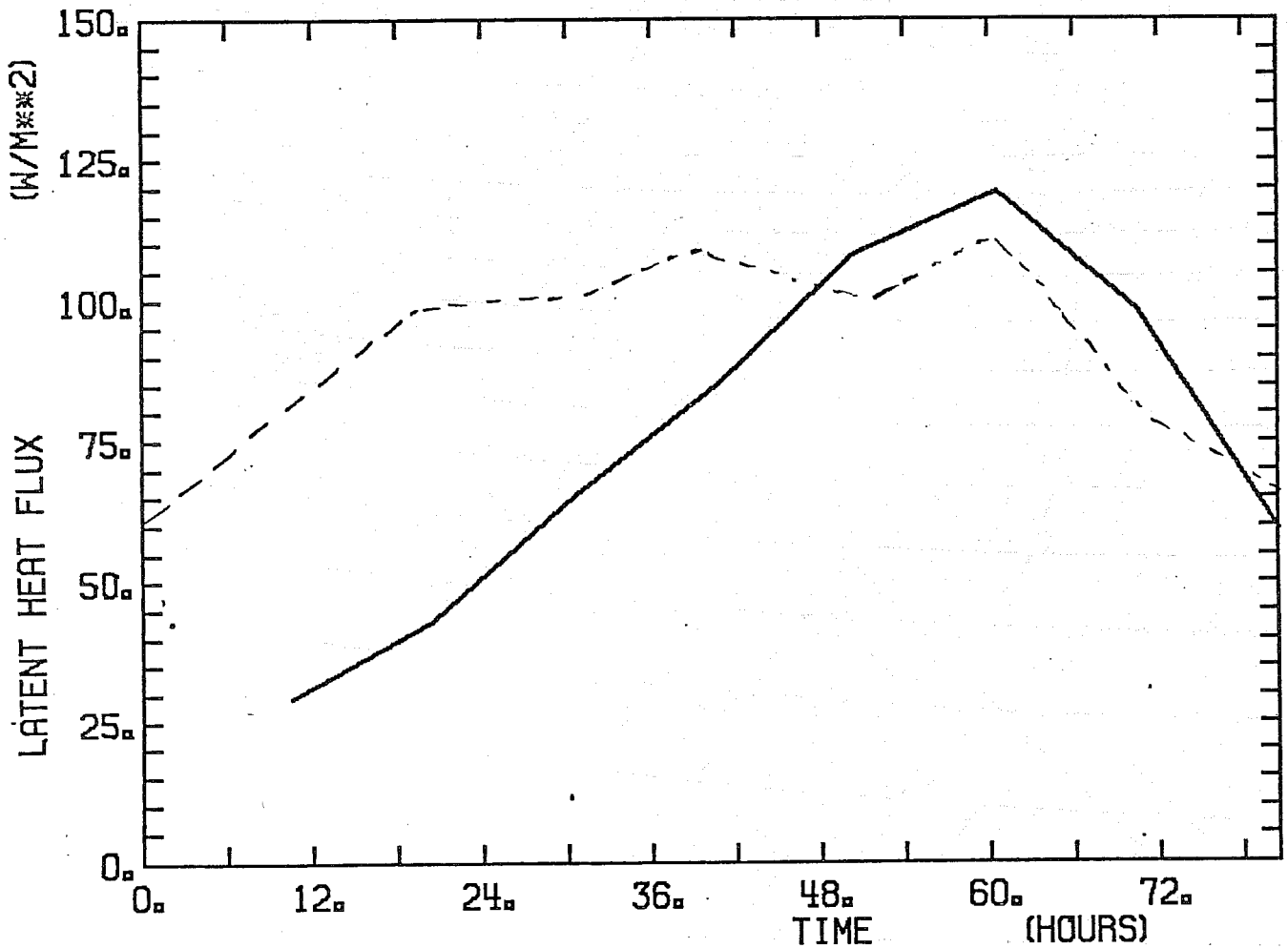

Fig. 23 Time evolution of surface flux of latent heat in GATE experiment 3 (observed values are dashed).

cumulus clouds, where they vanish. In experiment 3 convective heating and moistening is prescribed.

The results of the integrations are only briefly summarized (Figs. 19-22). The experiment, where both turbulent fluxes and convection is parameterized, predicted an atmosphere several K colder than observed (Fig. 1a), which is due to an underestimate of convective heating. The surface fluxes of heat and moisture are also much smaller in the simulation (Fig. 20). In order to see if the lack of convective heating is directly related to the underestimated surface fluxes, experiments 2 and 3 were performed. Experiment 2, where the surface fluxes are prescribed, shows a remarkably good agreement between predicted and verified temperatures, although the moisture content is too high in the upper half of the troposphere and too low in the lower half (Fig. 21). Forecast and verification also agree well in the boundary layer. The third simulation, where only the turbulent fluxes of moisture and heat are parameterized, gave larger and more realistic surface fluxes (Fig. 23) than the first simulation, but there are still deficiencies in the predicted boundary layer moisture content, which is too low, particularly at the lowest level (Fig. 22).

In summary, we may conclude from these experiments that the interface between the boundary layer flow and the convective flow is probably erroneous in the EC-model and can lead to overall errors in temperature.

Three case studies are presented here. A further case which represents the diurnal variation of boundary layer structure under clear sky has been described by Louis (1979). More case studies, which are relevant to various synoptical situations such as the disturbed and undisturbed tradewinds, are planned.

REFERENCES

Arakawa, A. and W.H. Schubert. 1974. Interaction of a cumulus cloud ensemble with the large-scale environment, Part I. J. Atmos. Sci., 31, 674-701.

Augstein, E. 1978. The atmospheric boundary layer over the tropical oceans. Meteorology over the tropical oceans, Roy. Met. Soc., pp. 73-103.

Augstein, E., H. Riehl, F. Ostapoff and V. Wagner. 1973. Mass and Energy Transports in an Undisturbed Atlantic Tradewind Flow. Mon. Wea. Rev., 101, 101-111.

Carson, D.F. 1977. Characteristics of the near-neutral boundary layer derived from the Leipzig wind profile data. Met. O 20, Technical Note No. II/104, Meteorological Office, Bracknell, U.K.

Han, Y-F. and S-W. Lee. 1981. A new Analysis of monthly mean wind stress over the global ocean. Available from Oregon State University, Corvallis, U.S.A.

Hastenrath, S. and P.F. Lamb. 1977. Climatic Atlas of the Tropical Atlantic and Eastern Pacific Oceans. The Univ. of Wisconsin Press.

———————— 1978. Heat Budget Atlas of the Tropical Atlantic and Eastern Pacific Oceans. Univ. of Wisconsin Press.

———————— 1979. Climatic Atlas of the Indian Ocean.
Part 1: Surface Climate and Atmospheric Circulation.
Part 2: The Oceanic Heat Budget. The Univ. of Wisconsin Press.

Hsu, S-A. 1973. Dynamics of the Sea Breeze in the Atmospheric Boundary Layer - A case study of the Free Convection Regime. Mon. Wea. Rev., 101, 187-194.

Hellerman, S. 1967. An updated estimate of the wind stress on the world ocean. Mon. Wea. Rev., 95, 607-626 (Convection, Mon. Wea. Rev., 96, 63-74).

Jenne, R.L., H.L. Crutcher, H. van Loon, T.J. Taljaard. 1971. Climate of the Upper Air: Southern Hemisphere, Vol. III. Vector mean geostrophic winds. NCAR TN/STR-58.

Lettan, H. 1950. A re-examination of the "Leipzig Wind Profile" considering some relations between wind and turbulence in the frictional layer. Tellus, 2, 125-129.

Louis, J-F. 1979. A parametric model of vertical eddy fluxes in the atmosphere. Boundary Layer Meteorology, 17, 187-202.

Mildner, P. 1932. Uber die Rebung in einer spexelen Luftmasse in den imtersten schiditen der Atmosphäre. Beitr. Phys. fr. Atmos., 19, 151-158.

Ninomiya, K. 1977. Heat and water-vapour budget over the East China Sea in the Winter season. Collected Scientific Papers of the AMTEX, No. 1. Japanese National Committee for GARP, 59-91.

Ninomiya, K. and T. Akiyama, 1976. Structure and Heat Energy Budget of Mixed Layer capped by Inversion during the period of Polar outbreak over Kuroshio Region. J. Met. Soc. Japan, 54, 160-174.

Pruitt, W.O., D.L. Morgan and F.J. Lonvence. 1973. Momentum and mass transfers in the surface boundary layer. Q.J.R. Met. Soc., 99, 370-386.

Riehl, H. et al., 1951. The North-east Trade of the Pacific Ocean. Q.J.R. Met.Soc., 77, 598-626.

Riehl, H. and J.S. Malkus. 1957. On the heat balance and maintenance of circulation in the trades. Q.J.R.Met.Soc., 83, 21-29.

Thompson, R.M., S.W. Payne, E.E. Reeker and R.J. Reed. 1979. Structure and properties of synoptic-scale wave disturbances in the intertropical convergence zone of the eastern Atlantic. J.Atmos.Sci., 36, 53-72.

Tiedtke, M., J-F. Geleyn, A. Hollingsworth, J-F. Louis. 1979. ECMWF model, parameterization of subgrid scale processes. ECMWF Technical Report No. 10.

Tiedtke, M. 1980. Diagnostics of diabatic processes in global numerical experiments at ECMWF. Proceedings of Workshop on Diagnostics of diabatic processes, at ECMWF, 23-25 April 1980, pp. 135-152.